Disclike vs. cylindrical micelles: Generalized model of micelle growth and data interpretation

Svetoslav E. Anachkov [a], Peter A. Kralchevsky [a,*], Krassimir D. Danov [a], Gergana S. Georgieva [a], Kavssery P. Ananthapadmanabhan [b]

[a] Department of Chemical Engineering, Faculty of Chemistry and Pharmacy, Sofia University, Sofia 1164, Bulgaria
[b] Unilever Research & Development, 40 Merritt Blvd., Trumbull, CT 06611, USA

ARTICLE INFO

ABSTRACT

Here, we present a detailed theoretical model describing the growth of disclike surfactant micelles. The model is tested against light-scattering data for micellar solutions from mixed conventional surfactants and from fluorinated surfactants. Theoretical expressions are derived for the concentration dependencies of the number and mass average aggregation numbers. Central role in the theory is played by the difference between the chemical potentials of a surfactant molecule in cylindrical and discoidal micelles. This difference, scaled with the thermal energy kT, is denoted p. For $p < 0$, the formation of cylindrical (rather than disclike) micelles is energetically favored. For $p > 0$ disclike micelles are formed, but their growth is limited due to the rise of their positive peripheral energy. Because of that, disclike micelles can be observed in a relatively narrow interval, $0 < p < 0.1$, and in a limited concentration range. Three sets of light-scattering data for different surfactants were processed. It is remarkable that in all cases the best fit gives small positive values of p, in agreement with the theoretical predictions. The model predicts that a strong increase in the viscosity of a surfactant solution should happen upon the transformation of disclike micelles into cylindrical ones at small variations in p. The model can be used for analyzing the shape and size of micelles in various surfactant solutions. The fact that typical disclike micelles form only in the special case $0 < p < 0.1$ shows why such micelles represent a relatively rare form of stable surfactant self-assembly.

1. Introduction

Disclike micelles from amphiphilic molecules, called also nanodiscs or bicelles, represent a relatively rare form of self-assemblies as compared to the cylindrical (rodlike, wormlike) micelles [1,2]. Nevertheless, discoidal aggregates have been observed in numerous studies. *Single* component disclike micelles were found in solutions of some anionic [3] and nonionic [4] surfactants, fluorinated surfactants [5–8], and with the protein β-casein [4]. After the pioneering works by Eastoe et al. [9] and Zemb et al. [1], nanodiscs were detected and investigated in various *binary* mixtures of cationic and anionic (catanionic) surfactant solutions [10–13]. Disc-shaped micelles and nematic phase from such micelles were observed in *ternary* mixtures of anionic and zwitterionic surfactant plus lauric acid [14]. Discoidal aggregates are formed also in solutions of diblock and triblock copolymers [15–20]. Such aggregates have been discovered in solutions of bile salts [21–23] and their mixtures with phospholipids [24]. Disclike micelles are formed also by phospholipids dispersed in water [25,26] and in aqueous surfactant/lipid systems [27]. The self-assembly of discoidal aggregates has been found to be a transitional kinetic stage in the processes of formation and decomposition of liposomes [28,29].

At higher concentrations, the cylindrical micelles give rise to columnar organisations such as columnar nematic, and columnar hexagonal and rectangular phases. Likewise, disc-shaped micelles can form nematic discotic and lamellar L_α phases [30–32]. It was established that the size of the cylindrical aggregates increases continuously with concentration, while the size of the discs could jump from small to infinite [33,34]. The phase transitions between isotropic and columnar phases (for rodlike micelles), as well as between isotropic and lamellar phases (for disclike micelles) have been theoretically studied [35].

Shape polydispersity and shape fluctuations in ionic surfactant micelles were analyzed theoretically on the basis of a model for the free energy of deformation, which leads to transitions from spherical micelles to prolate and oblate ellipsoids [36]. Such transitions have been predicted also by computer simulations [37]. The formation of cylindrical and disclike micelles and their transformation into liquid crystalline phases was theoretically described in terms

* Corresponding author. Fax: +359 2 9625643.
  E-mail address: pk@lcpe.uni-sofia.bg (P.A. Kralchevsky).

of the Helfrich curvature moduli [38,39] and lattice Hamiltonian models [33]. For cylindrical micelles, there are molecular–thermodynamic models, coupled with geometrical-constraint considerations, which quantitatively predict the micelle growth with the rise of surfactant concentration [40–42]. Surprisingly, such models are missing for disclike micelles.

Our goals in the present article are (i) to develop a molecular–thermodynamic model of disclike micelles that quantitatively describes the variation in the micelle size with the increase of surfactant concentration; (ii) to test the model against experimental results for disclike micelles, which includes development of a procedure for determining the model parameters by data fits, and (iii) to discuss the predictions of the model regarding the transitions from disclike to cylindrical micelles and vice versa. We take into account the main difference between the rodlike and disclike micelles, viz. that the size of the hemispherical caps of the rod is independent of micellar length, whereas the size of the semitoroidal rim around the disc increases with its diameter.

The paper is organized as follows. In Section 2, we briefly present the ladder model of the growth of cylindrical micelles by Missel et al. [41], in view of its subsequent extension to discoidal aggregates. In Section 3, the model is extended to multi-component micelles. In Section 4 the geometrical relations for spherical, cylindrical and disclike micelles are derived and compared. In Section 5, theoretical expressions for the experimentally measurable radius of gyration, R_g, and hydrodynamic radius, R_h, are derived for *toro-disc* shaped micelles. The molecular–thermodynamic model of disclike micelles is developed in Section 6, where an expression for the micelle size distribution is derived, and it is applied to obtain equations for calculating the micelle number and mass average aggregation numbers, $\bar{n}_N$, and $\bar{n}_M$. The comparison of the free energies of solutions with cylindrical and disclike micelles reveals the domains where the formation of these differently shaped aggregates is energetically favorable. In Section 7, we consider the limitations on the growth of disclike micelles, derive corresponding theoretical expressions and discuss their numerical predictions. Finally, in Sections 8 and 9 the model is tested against data for conventional and fluorinated surfactants, and its predictions regarding the transitions from disclike to cylindrical micelles, and vice versa, are discussed. The proposed model predicts the laws of growth of discoidal aggregates and reveals why disclike micelles are less frequently observed in comparison with the cylindrical ones.

2. The "ladder model" for single-component cylindrical micelles

Here, we briefly present the ladder model by Missel et al. [41] in view of its subsequent generalization to mixed and disclike micelles. The model describes the growth of cylindrical micelles. First, it was applied to ionic surfactants, such as sodium dodecyl sulfate (SDS) in the presence of a fixed high concentration of NaCl, at which the electrostatic interactions are suppressed. The model was further generalized to the cases of ionic surfactants in the presence of 2:1 ($CaCl_2$) and 3:1 ($AlCl_3$) electrolytes taking into account the contribution of electrostatic interactions [43–45]. Here, the model is presented in its version for nonionic surfactants and the next terms in the series expansions for the number and mass average aggregation numbers, $\bar{n}_N$ and $\bar{n}_M$, are derived.

2.1. Basic thermodynamic relationships

The chemical equilibrium between the micelles of aggregation number n and the free surfactant monomers is described by the equation:

$$n\mu_1 = \mu_n \tag{2.1}$$

where μ_1 and μ_n are the chemical potentials of the monomers and the micelles, respectively. Assuming an ideal solution, from Eq. (2.1) we obtain:

$$n\widetilde{\mu}_1 + nkT\ln X_1 = \widetilde{\mu}_n + kT\ln X_n \tag{2.2}$$

where $\widetilde{\mu}_1$ and $\widetilde{\mu}_n$ are standard chemical potentials; X_1 and X_n are the molar fractions of monomers and micelles of aggregation number n in the solution; k is the Boltzmann constant; T is the absolute temperature. X_1 is close to the critical micellization concentration (CMC), expressed in terms of molar fraction. Taking inverse logarithm of Eq. (2.2), we obtain an expression for the micelle size distribution [41]:

$$X_n = X_1^n \exp\left(-\frac{\widetilde{\mu}_n - n\widetilde{\mu}_1}{kT}\right) \tag{2.3}$$

2.2. Basic assumption of the ladder model

Assuming that the standard chemical potential of the cylindrical micelle is a sum of contributions from its cylindrical part and from its two hemispherical caps (Fig. 1), we obtain [41]:

$$\widetilde{\mu}_n = \bar{\mu}^{(c)}(n - n_s) + \bar{\mu}^{(s)}n_s \tag{2.4}$$

Here, $\widetilde{\mu}^{(s)}$ and $\widetilde{\mu}^{(c)}$ are the standard chemical potentials of surfactant molecules in the spherical and cylindrical parts of a micelle, respectively; n is the total number of surfactant molecules contained in the micelle, whereas n_s is the total number of surfactant molecules contained in the two hemispherical caps (Fig. 1). From Eq. (2.4), we obtain:

$$\widetilde{\mu}_n - n\widetilde{\mu}_1 = (\widetilde{\mu}^{(s)} - \widetilde{\mu}^{(c)})n_s + (\widetilde{\mu}^{(c)} - \widetilde{\mu}_1)n \tag{2.5}$$

The substitution of Eq. (2.5) into Eq. (2.3) yields [41]:

$$X_n = \frac{1}{K}\left(\frac{X_1}{X_B}\right)^n, \quad \frac{X_1}{X_B} < 1, n \geqslant n_s \tag{2.6}$$

where

$$K = \exp\left(\frac{n_s(\widetilde{\mu}^{(s)} - \widetilde{\mu}^{(c)})}{kT}\right) \tag{2.7}$$

$$X_B = \exp\left(\frac{\widetilde{\mu}^{(c)} - \widetilde{\mu}_1}{kT}\right) \tag{2.8}$$

Eq. (2.6) represents the micelle size-distribution for $n \geqslant n_s$. In particular, $n = n_s$ corresponds to the smallest spherical micelles. Eq. (2.6) implies that with the growth of n, the concentration X_n of the micelles exponentially decreases with the rise of the aggregation number n. The total (input) molar fraction of surfactant in the solution is:

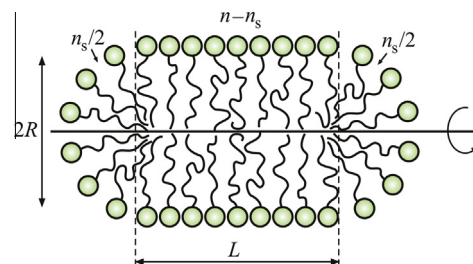$$X = X_1 + \sum_{n=n_s}^{\infty} nX_n \tag{2.9}$$

Fig. 1. Sketch of a cylindrical micelle with two hemispherical caps; n is the total number of surfactant molecules contained in the micelle; n_s is the total number of surfactant molecules contained in the two hemispherical caps.

The series in Eq. (2.9) must be convergent, and consequently we must have $X_1/X_B < 1$. The substitution of Eq. (2.6) into Eq. (2.9) yields:

$$X = X_1 + \frac{1}{K}\sum_{n=n_s}^{\infty} n q^n, \quad q \equiv \frac{X_1}{X_B} < 1 \tag{2.10}$$

Eq. (2.10) can be represented in the form:

$$K(X - X_1) = \sum_{n=n_s}^{\infty} n q^n = \sum_{n=n_s}^{\infty} [n_s q^n + (n - n_s)q^n] \tag{2.11}$$

The first term in the brackets expresses the contribution from the hemispherical caps, whereas the second term is the contribution from the micelle cylindrical part (Fig. 1). The summation in Eq. (2.11) leads to:

$$K(X - X_1) = q^{n_s}\frac{n_s}{1-q} + q^{n_s}\frac{q}{(1-q)^2} \tag{2.12}$$

As above, the two terms in the right hand side of Eq. (2.12) represent, respectively, contributions from the hemispherical caps and from the cylindrical parts of the micelles. If large cylindrical (rod-like or wormlike) micelles are present in the solution, then the last term in Eq. (2.12) must be predominant:

$$\frac{q}{(1-q)^2} \gg \frac{n_s}{1-q} \Rightarrow \varepsilon \equiv 1 - q \ll 1 \tag{2.13}$$

In terms of the small parameter ε, Eq. (2.12) acquires the form:

$$K(X - X_1) = (1 - \varepsilon)^{n_s}\left(\frac{n_s}{\varepsilon} + \frac{1-\varepsilon}{\varepsilon^2}\right) \tag{2.14}$$

Because small ε corresponds to large micelles and large $K(X - X_1)$, from Eq. (2.14) we can express $1/\varepsilon$ in the form of an asymptotic expansion for large $K(X - X_1)$:

$$\frac{1}{\varepsilon} = [K(X - X_1)]^{1/2} + \frac{1}{2} + \frac{1 + 2n_s(n_s - 1)}{8[K(X - X_1)]^{1/2}}$$
$$+ O\left\{[K(X - X_1)]^{-3/2}\right\} \tag{2.15}$$

2.3. Expression for the mean aggregation number

By definition, the *number-average* micelle aggregation number is:

$$\bar{n}_N = \left(\sum_{n=n_s}^{\infty} n X_n\right) \bigg/ \left(\sum_{n=n_s}^{\infty} X_n\right) \tag{2.16}$$

In view of Eqs. (2.6), (2.9), and (2.10), the summation in Eq. (2.16) yields [41]:

$$\bar{n}_N = \frac{1}{\varepsilon} + n_s - 1 \quad \text{(cylindrical micelles)} \tag{2.17}$$

Eqs. (2.14) and (2.17) give the dependence of $\bar{n}_N$ on the total surfactant concentration, X, in a parametric form: $X = X(\varepsilon)$ and $\bar{n}_N = \bar{n}_N(\varepsilon)$. An approximate asymptotic expression for the dependence $\bar{n}_N(X)$ at large $K(X - X_1)$ can be obtained by substituting Eq. (2.15) into Eq. (2.17):

$$\bar{n}_N = [K(X - X_1)]^{1/2} + n_s - \frac{1}{2} + \frac{1 + 2n_s(n_s - 1)}{8[K(X - X_1)]^{1/2}}$$
$$+ O\left\{[K(X - X_1)]^{-3/2}\right\} \tag{2.18}$$

Because the first term in the right-hand side is the leading one, the plot of $\bar{n}_N$ vs. $(X - X_1)^{1/2}$ must be a straight line with slope $K^{1/2}$ [41].

By definition the *mean mass* micelle aggregation number is:

$$\bar{n}_M = \left(\sum_{n=n_s}^{\infty} n^2 X_n\right) \bigg/ \sum_{n=n_s}^{\infty} n X_n \tag{2.19}$$

In view of Eqs. (2.6), (2.9), and (2.10), the summation in Eq. (2.19) yields [41]:

$$\bar{n}_M = \frac{2}{\varepsilon} - 1 + \frac{n_s(n_s - 1)\varepsilon}{1 + (n_s - 1)\varepsilon} \quad \text{(cylindrical micelles)} \tag{2.20}$$

Eqs. (2.14) and (2.20) give the dependence of $\bar{n}_M$ on the total surfactant concentration, X, in a parametric form: $X = X(\varepsilon)$ and $\bar{n}_M = \bar{n}_M(\varepsilon)$. An approximate asymptotic expression for the dependence $\bar{n}_M(X)$ at large $K(X - X_1)$ can be obtained by substituting Eq. (2.15) into Eq. (2.20) and expanding in series:

$$\bar{n}_M = 2[K(X - X_1)]^{1/2} + \frac{1 + 6n_s(n_s - 1)}{4[K(X - X_1)]^{1/2}} + O\left(\frac{1}{K(X - X_1)}\right) \tag{2.21}$$

The first term in the right-hand side is the leading one, so that the plot of $\bar{n}_M$ vs. $(X - X_1)^{1/2}$ must be a straight line with slope $2K^{1/2}$ [41]. The comparison of Eqs. (2.18) and (2.21) shows that for large cylindrical micelles we have $\bar{n}_M/\bar{n}_N \approx 2$, as first established by Mukerjee [46]. The leading-term square-root dependence in Eq. (2.21) was confirmed in Ref. [43] for cylindrical micelles formed in aqueous solutions of the anionic surfactant sodium laurylethersulfate with two ethylene-oxide groups (SLES-2EO) with 0.7 M added NaCl.

3. Generalization of the ladder model for multi-component systems

3.1. General thermodynamic relations

Here, we generalize the model from Ref. [41] for multi-component systems, like that considered in Section 8.1. As before, we assume that the solution contains surfactant monomers and micelles of total aggregation number $n \geq n_s$, where n_s corresponds to the smallest spherical micelles. Let us assume that all micellar aggregates have the *same* composition, irrespective of their size:

$$(y_1, y_2, \ldots, y_N), \quad \sum_{i=1}^{N} y_i = 1 \tag{3.1}$$

where $y_1, \ldots, y_N$ are molar fractions. Because the micelles are polydisperse, the above assumption means that the composition in the central part of the micelle and in its curved periphery is the same. In other words, we have assumed that the curvature driven component segregation within the micelles is negligible. If for a given system the segregation effect is considerable, this can be detected as a deviation of the predictions of the present model from the experiment.

At concentrations much higher than the CMC, the amount of surfactant in micellar form is much greater than in monomeric form. Then, the micelle composition $(y_1, y_2, \ldots, y_N)$ practically coincides with the composition of the input components, which is known. The following relationships hold:

$$n_i = n y_i, \quad \sum_{i=1}^{N} n_i = n \sum_{i=1}^{N} y_i = n \tag{3.2}$$

where n_i is the number of molecules from the component "i" in a micelle of total aggregation number n. The chemical potential of the monomers in the solution is:

$$\mu_i^{(1)} = \tilde{\mu}_i^{(1)} + kT \ln x_i \quad (i = 1, 2, \ldots, N) \tag{3.3}$$

where x_i is the concentration of the free monomers from the component "i". As before, the chemical potential of the micelles of aggregation number 'n' is:

$$\mu_n = \widetilde{\mu}_n + kT \ln X_n \quad (n \geqslant n_s) \tag{3.4}$$

At equilibrium, we have:

$$\sum_{i=1}^{N} n_i \mu_i^{(1)} = \mu_n \quad (n \geqslant n_s) \tag{3.5}$$

n_s is the total aggregation number of the spherical mixed micelles. The substitution of Eqs. (3.3) and (3.4) into Eq. (3.5), along with the relation $n_i = n y_i$, yields

$$\ln X_n = -\frac{\widetilde{\mu}_n - n\bar{\mu}^{(1)}}{kT} + n \ln \overline{X}_1 \quad (n \geqslant n_s), \tag{3.6}$$

where

$$\bar{\mu}^{(1)} = \sum_{i=1}^{N} y_i \widetilde{\mu}_i^{(1)} \quad \text{and} \quad \overline{X}_1 = \left(\prod_{i=1}^{N} x_i^{n_i}\right)^{1/n} \tag{3.7}$$

are, respectively, the mean arithmetic standard chemical potential of the free monomers, and their mean geometric molar fraction. So far, we did not make any assumptions concerning the micelle shape. Hence, Eqs. (3.6) and (3.7) are applicable to both cylindrical and disclike micelles.

3.2. Application to cylindrical micelles

For cylindrical micelles in *mixed* surfactant solutions, the basic assumption of the ladder model, Eq. (2.4), can be generalized in the following way:

$$\widetilde{\mu}_n = n_s \bar{\mu}^{(s)} + (n - n_s) \bar{\mu}^{(c)} \tag{3.8}$$

where $\bar{\mu}^{(s)}$ and $\bar{\mu}^{(c)}$ are the mean standard chemical potential of a surfactant molecule, respectively, in the spherical and cylindrical parts of a micelle of aggregation number n; see Fig. 1. With the help of Eq. (3.8), we obtain:

$$\widetilde{\mu}_n - n\bar{\mu}^{(1)} = n_s(\bar{\mu}^{(s)} - \bar{\mu}^{(c)}) + n(\bar{\mu}^{(c)} - \bar{\mu}^{(1)}) \tag{3.9}$$

Substituting Eq. (3.9) into Eq. (3.6) and taking inverse logarithm, we obtain the size distribution of the sphero-cylindrical micelles in the muli-component surfactant solution:

$$X_n = \frac{1}{K} \left(\frac{\overline{X}_1}{X_B}\right)^n (n \geqslant n_s) \tag{3.10}$$

where

$$K = \exp\left(\frac{n_s(\bar{\mu}^{(s)} - \bar{\mu}^{(c)})}{kT}\right), \quad X_B = \exp\left(\frac{\bar{\mu}^{(c)} - \bar{\mu}^{(1)}}{kT}\right) \tag{3.11}$$

The total molar fraction of the micelles is given again by Eq. (2.9), where the series must be convergent. Correspondingly, we should have $\overline{X}_1/X_B \equiv q < 1$. Then, using the same logical scheme as in Eqs. (2.10), (2.11), (2.12), (2.13), (2.14), (2.15), we arrive at the same expressions, Eqs. (2.18) and (2.21), for the number and mass average aggregation numbers of the micelles, $\bar{n}_N$ and $\bar{n}_M$, where

$$X_1 = \sum_{i=1}^{N} x_i \tag{3.12}$$

4. Geometric relations for micelles of different shape

4.1. Spherical micelles

For a spherical micelle, we have the following estimates:

$$n_s = \frac{\frac{4}{3}\pi R^3}{\bar{v}}, \quad a_s = \frac{4\pi R^2}{n_s} = \frac{3\bar{v}}{R} \tag{4.1}$$

n_s is the aggregation number of the spherical micelle; R is the radius of its hydrophobic core; a_s is the area per molecule relative to the surface of the hydrophobic core; $\bar{v}$ is the mean volume per hydrocarbon chain in the micelle. For a multi-component surfactant mixture, both R and $\bar{v}$ are average quantities:

$$R = \sum_{i=1}^{N} y_i l_i, \quad \bar{v} = \sum_{i=1}^{N} y_i v_i \tag{4.2}$$

y_i is the mole fraction of the amphiphilic component i in the mixed micelle; l_i is the length of the hydrocarbon chain of the respective molecule; v_i is the volume of the tail of a molecule of the ith component. The aggregation number n_s is:

$$n_s = \sum_{i=1}^{N} n_i^{(s)}, \quad y_i = \frac{n_i^{(s)}}{n_s} \tag{4.3}$$

where $n_i^{(s)}$ is the number of molecules from component i in the spherical micelle.

4.2. Cylindrical micelles

Here, we follow the model from Fig. 1, i.e. the cylindrical micelle consists of a cylinder of length L and two hemispherical caps of radius R equal to the cylinder's radius. As above, we assume that the cylindrical and hemispherical parts of the micelle have the same composition, i.e. y_i is the same ($i = 1, \ldots, N$). Then, Eqs. (4.1), (4.2), (4.3) hold again for the two hemispherical caps, which by size and aggregation number correspond to a spherical micelle. For the cylindrical part of the micelle, we have:

$$n_c = \frac{\pi R^2 L}{\bar{v}}, \quad a_c = \frac{2\pi R L}{n_c} = \frac{2\bar{v}}{R} \tag{4.4}$$

n_c is the aggregation number of the cylindrical part of the micelle; a_c is the area per molecule relative to the cylindrical part of the surface of the hydrophobic core. The aggregation number of the cylindrical part of the micelle n_c is:

$$n_c = \sum_{i=1}^{N} n_i^{(c)}, \quad \frac{n_i^{(c)}}{n_c} = \frac{n_i^{(s)}}{n_s} = y_i \tag{4.5}$$

where $n_i^{(c)}$ is the number of molecules from component i in the cylindrical part of the micelle.

4.3. Disclike micelles

In analogy with the cylindrical micelles, which are modeled as "sphero-cylinders", the disclike micelles can be modeled as "toro-discs", consisting of a disc of diameter L and thickness $2R$, and of a periphery that represents a semitorus of radius R (Fig. 2). The volume and the surface area of the disclike micelle can be expressed in the form:

$$V = V_d + V_t, \quad A = A_d + A_t \tag{4.6}$$

where the indices 'd' and 't' refer to the discoidal and toroidal parts of the micelle, respectively. The volume and the surface area of the discoidal part are:
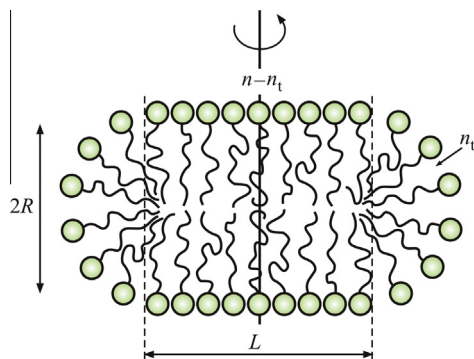
$$V_d = \frac{\pi}{2} R L^2, \quad A_d = \frac{\pi}{2} L^2 \tag{4.7}$$

Likewise, the volume and surface area of the toroidal periphery of the micelle are:

$$V_t = \frac{\pi^2}{2} R^2 L + \frac{4}{3} \pi R^3, \quad A_t = \pi^2 R L + 4\pi R^2 \tag{4.8}$$

(see Appendix A.1). The number of surfactant molecules n_d and the area a_d in the *discoidal part* of the micelle are as follows:

Fig. 2. Sketch of a disclike micelle with a semitoroidal periphery; n is the total number of surfactant molecules contained in the micelle, whereas n_t is the number of surfactant molecules belonging to the periphery.

$$n_d = \frac{V_d}{\bar{v}} = \frac{\pi R L^2}{2\bar{v}}, \quad a_d = \frac{\pi L^2}{2n_d} = \frac{\bar{v}}{R} \tag{4.9}$$

where Eq. (4.7) was used. Summarizing Eqs. (4.1), (4.4), and (4.9), we obtain:

$$a_d = \frac{\bar{v}}{R}, \quad a_c = \frac{2\bar{v}}{R}, \quad a_s = \frac{3\bar{v}}{R} \tag{4.10}$$

In other words, the area per molecule is the smallest for the discoidal part of a micelle and the largest for a spherical micelle.

For the *toroidal periphery* of the disclike micelle, in analogy with Eq. (4.9), using Eq. (4.8) we obtain:

$$n_t = \frac{V_t}{\bar{v}} = \frac{1}{\bar{v}} \left(\frac{\pi^2}{2} R^2 L + \frac{4}{3}\pi R^3 \right) \tag{4.11}$$

$$a_t = \frac{A_t}{n_t} = \frac{\pi L + 4R}{\pi L + \frac{8}{3}R} \frac{2\bar{v}}{R} \tag{4.12}$$

where n_t and a_t are, respectively, the total number of surfactant molecules and the area per molecule in the toroidal part of the disc-like micelle. Eq. (4.11) shows how the number of surfactant molecules in the toroidal part of the micelle increases with the micelle diameter L. In the limit $L = 0$, the "toro-disc" becomes a sphere, and Eq. (4.11) yields $n_t = n_s$; see Eq. (4.1).

The comparison of Eqs. (4.1), (4.4), and (4.12) leads to the following inequalities:

$$\frac{2\bar{v}}{R} = a_c \leqslant a_t \leqslant a_s = \frac{3\bar{v}}{R} \tag{4.13}$$

In other words, the area per molecule in the toroidal part of the micelle is greater than that for a cylindrical micelle, but smaller than that for a spherical micelle. Indeed, for large disclike micelles ($L \to \infty$), Eq. (4.12) yields $a_t \to a_c$, whereas for small disclike micelles ($L \to 0$), Eq. (4.12) yields $a_t \to a_s$. The inequalities in Eq. (4.13) will be essentially used in Section 6 to find the law of growth of the disclike micelles.

The expression $a_d = \bar{v}/R$ was obtained only on the basis of considerations about the radius and volume of the micelle hydrophobic core; see Eq. (4.2). This is possible only if the surfactant headgroups are relatively small. For the headgroups, we can define a_h as the average excluded area per headgroup at *close packing*. Apparently, we should have $a_d \geqslant a_h$, where we are dealing with areas projected on the surface of the micelle hydrophobic core. Then, the generalized definition of a_d is:

$$a_d = \begin{cases} \bar{v}/R & \text{for } \bar{v}/R > a_h \\ a_h & \text{for } \bar{v}/R \leqslant a_h \end{cases} \tag{4.14}$$

For mixed micelles, the average excluded area per headgroup at close packing, a_h, can be estimated from the expression:

$$a_h \approx \sum_{i=1}^{N} y_i a_{h,i} \tag{4.15}$$

where $a_{h,i}$ are excluded areas per headgroup of the pure component 'i' at close packing, projected on the surface of the hydrophobic core of the micelle. Eq. (4.15) corresponds to a *chaotic* mixing of headgroups of different kind and size. For a special *regular* ordering of the headgroups, a_h could have a minimal value [47].

5. Disclike micelles: radius of gyration and hydrodynamic radius

The *radius of gyration* of micelles, R_g, can be determined by *static* light scattering (or SANS) experiments, from the angular dependence of the scattered light (Guinier plot) [44,48]. In addition, the *hydrodynamic radius*, R_h, can be determined by *dynamic* light scattering, from data for the time autocorrelation function of the scattered light intensity [49]. Here, we consider the relations between R_g, R_h and the geometrical parameters of *toro-disc* shaped micelles: L – diameter of the discoidal part and b – radius of the semitoroidal periphery, see Fig. 3.

The parameter b includes contributions from the surfactant headgroup and hydrocarbon chain,

$$b = R + \delta_h \tag{5.1}$$

where R is given by Eq. (4.2), and δ_h is the headgroup diameter.

For a body of volume V and uniform mass density, the *radius of gyration* R_g can be calculated from the expression [48]:

$$R_g^2 = \frac{1}{V} \int_V |\mathbf{r}|^2 \mathrm{d}V \tag{5.2}$$

The origin of the position vector $\mathbf{r}$ is in the mass center of the body; $\mathrm{d}V$ is the volume element. For a toro-disc, the integral in Eq. (5.2) can be solved exactly; see Appendix A.2. As a result, the following expression for the radius of gyration of a *toro-disc* is obtained:

$$R_g^2 = \frac{L^2}{8} \frac{1 + 2\pi u + 56u^2/3 + 8\pi u^3 + 64u^4/5}{1 + \pi u + 8u^2/3} \tag{5.3}$$

where $u = b/L$ (see Fig. 3).

For an arbitrarily shaped micelle of volume V and uniform mass density, the *hydrodynamic radius* R_h can be estimated from the expression [24]:

$$\frac{1}{R_h} = \frac{2}{3V} \int_V \frac{1}{|\mathbf{r}|} \mathrm{d}V \tag{5.4}$$

The origin of the position vector $\mathbf{r}$ is in the mass center of the micelle, and $\mathrm{d}V$ is the volume element. For a toro-disc, the integral in Eq. (5.4) cannot be solved in terms of elementary functions. In Appendix A.3, we derived a simple and very accurate expression for the hydrodynamic radius R_h of a *toro-disc*, viz.

$$R_h \approx b + \frac{3}{8}L \tag{5.5}$$
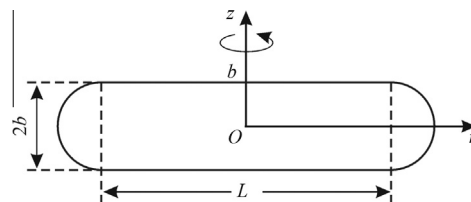
Fig. 3. Sketch of a toro-disc: $2b$ is simultaneously the thickness of the disc and the diameter of its semitoroidal periphery; L is the diameter of the central discoidal part.

The relative error of R_h calculated from Eq. (5.5) is smaller (by modulus) than 0.005 for all possible values of L/b; see Appendix A.3 for details.

Eqs. (5.3) and (5.5) can be used as a *criterion* to prove whether the micelles are *disclike* from experimental light scattering data for R_h and R_g. The parameter b is usually known – it is approximately equal to the length of the surfactant molecule, estimated from molecular-size considerations [42]. Then, from Eq. (5.5) we find $L = 8(R_h - b)/3$. Next, L is substituted in Eq. (5.3) to calculate R_g. If the calculated and measured R_g values are close, then the micelles are disclike.

6. Extension of the ladder model to disclike micelles

6.1. Size distribution of the disclike micelles

Our starting point is Eq. (3.6), which is applicable to both cylindrical and disclike micelles. First, we will obtain an expression for the arithmetic mean standard chemical potential of the micelle, $\tilde{\mu}_n$, that enters Eq. (3.6).

Insofar as the disclike micelle can be modeled as a combination of disc and torus (toro-disc, see Fig. 2), $\tilde{\mu}_n$ can be expressed in the form:

$$\tilde{\mu}_n = \bar{\mu}^{(d)}(n - n_t) + \bar{\mu}^{(t)}n_t \tag{6.1}$$

As before, n is the total aggregation number; n_t is the number of surfactant molecules in the semitoroidal periphery of the micelle; $\bar{\mu}^{(d)}$ and $\bar{\mu}^{(t)}$ are mean standard chemical potentials of a molecule that belongs, respectively, to the discoidal and toroidal part of the micelle. Eq. (6.1) for disclike micelles is analogous to Eq. (2.4) for cylindrical micelles. In the case of cylindrical micelles, the hemispherical caps are independent of the micelle length, L, whereas for disclike micelles the area per molecule in the toroidal periphery, a_t, depends on L; see Eq. (4.12). For this reason, $\bar{\mu}^{(s)}$ and n_s in Eq. (2.4) are independent of L, whereas in Eq. (6.1) both $\bar{\mu}^{(t)}$ and n_t depend on L. To take into account the aforementioned dependence, in Eq. (6.1) we expand $\bar{\mu}^{(t)}$ in series around $a = a_s$:

$$\tilde{\mu}_n = \bar{\mu}^{(d)}n + (\bar{\mu}^{(t)} - \bar{\mu}^{(d)})n_t$$
$$\approx \bar{\mu}^{(d)}n + \left[\bar{\mu}^{(s)} + \frac{\partial \bar{\mu}}{\partial a}\bigg|_{a=a_s}(a_t - a_s) - \bar{\mu}^{(d)}\right]n_t \tag{6.2}$$

Because $a_c \leqslant a_t \leqslant a_s$, the derivative in Eq. (6.2) can be estimated as follows:

$$\frac{\partial \bar{\mu}}{\partial a}\bigg|_{a=a_s} \approx \frac{\bar{\mu}^{(s)} - \bar{\mu}^{(c)}}{a_s - a_c} = (\bar{\mu}^{(s)} - \bar{\mu}^{(c)})\frac{R}{\bar{\nu}} \tag{6.3}$$

where the relation $a_s - a_c = \bar{\nu}/R$ has been used; see Eq. (4.10). In Appendix A.4, it is shown that the substitution of Eq. (6.3) into Eq. (6.2), along with some geometrical relations from Section 4, leads to the result:

$$\tilde{\mu}_n - n\bar{\mu}^{(1)} \approx (\bar{\mu}^{(s)} - \bar{\mu}^{(d)})n_s + (\bar{\mu}^{(d)} - \bar{\mu}^{(1)})n$$
$$- (\bar{\mu}^{(d)} - \bar{\mu}^{(c)})\frac{3\pi L}{8R}n_s \tag{6.4}$$

The estimate of the derivative in Eq. (6.3) is equivalent to *linear* interpolation of the dependence $\bar{\mu}(a_t)$ for $a_c \leqslant a_t \leqslant a_s$, see Eq. (4.13). For this reason, Eq. (6.4) is independent of whether an expansion around a_s [as in Eq. (6.2)], or around a_c is used.

The substitution of Eq. (6.4) in Eq. (3.6) leads to the following expression for the size distribution of the disclike micelles:

$$X_n = \frac{1}{K}\left(\frac{\bar{X}_1}{X_B}\right)^n \exp\left(\frac{\bar{\mu}^{(d)} - \bar{\mu}^{(c)}}{kT}\frac{3\pi L}{8R}n_s\right) \tag{6.5}$$

where

$$K \equiv \exp\left(\frac{\bar{\mu}^{(s)} - \bar{\mu}^{(d)}}{kT}n_s\right) \tag{6.6}$$

$$X_B \equiv \exp\left(\frac{\bar{\mu}^{(d)} - \bar{\mu}^{(1)}}{kT}\right) \tag{6.7}$$

Furthermore, it is convenient to introduce the dimensionless quantities x, ε and p as follows:

$$x = \frac{L}{R}, \quad \frac{\bar{X}_1}{X_B} = \exp(-\varepsilon) \tag{6.8}$$

$$p = \frac{\bar{\mu}^{(c)} - \bar{\mu}^{(d)}}{kT} \tag{6.9}$$

Then, Eq. (6.5) acquires the form:

$$X_n = \frac{1}{K}\exp\left(-\varepsilon n - \frac{3\pi}{8}n_s px\right) \tag{6.10}$$

For $p = 0$, Eq. (6.10) is mathematically identical to the respective expression for cylindrical micelles, Eq. (2.6). The term with p in Eq. (6.10) accounts for the increment of the excess peripheral energy of the disclike micelle. For positive/negative p, the peripheral energy increases/ decreases with the rise of disc diameter. The quantities n and x are not independent. Combining Eqs. (4.1), (4.9), and (4.11), we obtain:

$$n = n_d + n_t = \frac{3n_s}{8}x^2 + \frac{3n_s}{8}\pi x + n_s \tag{6.11}$$

In view of Eq. (6.11), it is convenient to represent the micelle size distribution, Eq. (6.10) in the form:

$$X_n = \frac{1}{K}\exp\left[F(x) - \frac{8}{3}\varepsilon_s\right]$$
$$F(x) \equiv -\varepsilon_s x^2 - \pi(p_s + \varepsilon_s)x \tag{6.12}$$

where

$$\varepsilon_s \equiv \frac{3n_s}{8}\varepsilon \text{ and } p_s \equiv \frac{3n_s}{8}p \tag{6.13}$$

6.2. Expression for the total surfactant molar fraction

The total surfactant molar fraction X is given by Eq. (2.9). In view of Eq. (6.12), it is convenient to replace the summation by integration using the Euler–Maclaurin formula (see Appendix A.5 for details):

$$X - X_1 = \sum_{n=n_s}^{\infty} nX_n \approx \frac{n_s X_{n_s}}{2} + \int_{n_s}^{\infty} nX_n dn \tag{6.14}$$

Substituting n and X_n from Eq. (6.11) and (6.12) in Eq. (6.14), we obtain:

$$K(X - X_1) = \left(\frac{3n_s}{8}\right)^2 \exp\left(-\frac{8\varepsilon_s}{3}\right)\left(\frac{32}{9n_s} + J_1\right) \tag{6.15}$$

$$J_1 \equiv \int_0^{\infty}\left(x^2 + \pi x + \frac{8}{3}\right)(2x + \pi)\exp[F(x)]dx \tag{6.16}$$

Substituting $F(x)$ from Eq. (6.12), we solve analytically the above integral:

$$J_1 = \frac{3\pi^2 p_s(p_s - \varepsilon_s) + 4\varepsilon_s(3 + 8\varepsilon_s)}{12\varepsilon_s^3}$$
$$- \frac{3\pi^2(p_s^2 - \varepsilon_s^2) + 2\varepsilon_s(9 + 16\varepsilon_s)}{24\varepsilon_s^{7/2}}p_s\pi^{3/2}(1 - erf\,\xi)\exp(\xi^2) \tag{6.17}$$

where $erf\,\xi$ is the conventional error function, and

$$\xi \equiv \frac{\pi(p_s + \varepsilon_s)}{2\varepsilon_s^{1/2}} \tag{6.18}$$

6.3. Number average aggregation number of disclike micelles

The number average aggregation number $\bar{n}_N$ is defined by Eq. (2.16). The numerator in this equation is given by Eq. (6.14), whereas the denominator can be estimated as follows:

$$\sum_{n=n_s}^{\infty} X_n \approx \frac{X_{n_s}}{2} + \int_{n_s}^{\infty} X_n dn = \frac{X_{n_s}}{2} + \int_{0}^{\infty} X_n(x) dn(x) \tag{6.19}$$

Here, the sum was replaced by integral using again the Euler–Maclaurin formula (Appendix A.5). As a result, using Eqs. (6.11) and (6.12) we obtain:

$$\sum_{n=n_s}^{\infty} X_n = \frac{1}{K} \frac{3n_s}{8} \exp\left(-\frac{8\varepsilon_s}{3}\right)\left(\frac{4}{3n_s} + J_0\right) \tag{6.20}$$

$$J_0 \equiv \int_{0}^{\infty} (2x + \pi) \exp[F(x)] dx \tag{6.21}$$

Substituting $F(x)$ from Eq. (6.12), we solve analytically the above integral:

$$J_0 = \frac{1}{\varepsilon_s} - \frac{p_s}{2}\left(\frac{\pi}{\varepsilon_s}\right)^{3/2}(1 - erf\,\xi)\exp(\xi^2) \tag{6.22}$$

Thus, the expression for $\bar{n}_N$ acquires the form:

$$\bar{n}_N = \frac{3n_s}{8}\left(\frac{32}{9n_s} + J_1\right)\Big/\left(\frac{4}{3n_s} + J_0\right) \tag{6.23}$$

where J_1 and J_0 are given by Eqs. (6.17) and (6.22). Eqs. (6.15) and (6.23) determine the concentration dependence of the number average aggregation number, $\bar{n}_N(X)$, in a parametric form, viz. $X = X(\varepsilon_s)$ and $\bar{n}_N = \bar{n}_N(\varepsilon_s)$.

6.4. Mass average aggregation number of disclike micelles

The mass average aggregation number $\bar{n}_M$ is defined by Eq. (2.19). The denominator in this equation is given by Eq. (6.14), whereas the numerator can be estimated as follows:

$$\sum_{n=n_s}^{\infty} n^2 X_n \approx \frac{n_s^2 X_{n_s}}{2} + \int_{n_s}^{\infty} n^2 X_n dn$$
$$= \frac{1}{K}\left(\frac{3n_s}{8}\right)^3 \exp\left(-\frac{8\varepsilon_s}{3}\right)\left(\frac{256}{27n_s} + J_2\right) \tag{6.24}$$

$$J_2 \equiv \int_{0}^{\infty} \left(x^2 + \pi x + \frac{8}{3}\right)^2 (2x + \pi)\exp[F(x)] dx \tag{6.25}$$

Substituting $F(x)$ from Eq. (6.12), we solve analytically the above integral:

$$J_2 = \frac{1}{144\varepsilon_s^5}\Big[9\pi^4 p_s^3(p_s - \varepsilon_s) + 162\pi^2 p_s^2\varepsilon_s + 3\pi^2(64$$
$$- 3\pi^2)p_s^2\varepsilon_s^2 - 126\pi^2 p_s\varepsilon_s^2 - 3\pi^2(64 - 3\pi^2)p_s\varepsilon_s^3$$
$$+ 32\varepsilon_s^2(9 + 24\varepsilon_s + 32\varepsilon_s^2)\Big] - \frac{p_s\pi^{3/2}}{288\varepsilon_s^{11/2}}[9\pi^4 p_s^4$$
$$+ 180\pi^2 p_s^2\varepsilon_s + 6\pi^2(32 - 3\pi^2)p_s^2\varepsilon_s^2 + 540\varepsilon_s^2 + 36(32$$
$$- 3\pi^2)\varepsilon_s^3 + (32 - 3\pi^2)^2\varepsilon_s^4](1 - erf\,\xi)\exp(\xi^2) \tag{6.26}$$

Thus, the expression for $\bar{n}_M$ acquires the form:

$$\bar{n}_M = \frac{3n_s}{8}\left(\frac{256}{27n_s} + J_2\right)\Big/\left(\frac{32}{9n_s} + J_1\right) \tag{6.27}$$

where J_1 and J_2 are given by Eqs. (6.17) and (6.26). Eqs. (6.15) and (6.27) determine the concentration dependence of the mass average aggregation number, $\bar{n}_M(X)$, in a parametric form, viz. $X = X(\varepsilon_s)$ and $\bar{n}_M = \bar{n}_M(\varepsilon_s)$.

6.5. Mean standard chemical potential of a surfactant molecule in the micelles

In Section 6.1, to derive the size distribution of disclike micelles we assumed that an universal dependence, $\bar{\mu} = \bar{\mu}(a)$, of the micelle mean standard chemical potential, $\bar{\mu}$, on the area per headgroup, a, exists. As usual, a is the average area per surfactant molecule projected on the surface of the micelle hydrophobic core. For a multi-component micelle, $\bar{\mu}$ can be defined as follows:

$$\bar{\mu} = \sum_{i=1}^{N} y_i \mu_i^{(mic)} \tag{6.28}$$

where y_i and $\mu_i^{(mic)}$ are the molar fractions and chemical potentials of the surfactant molecules from component 'i' within the micelles. The quantities $\bar{\mu}^{(d)}$, $\bar{\mu}^{(c)}$ and $\bar{\mu}^{(s)}$ in Eq. (6.4) can be defined as follows:

$$\bar{\mu}^{(d)} \equiv \bar{\mu}(a_d), \quad \bar{\mu}^{(c)} \equiv \bar{\mu}(a_c), \quad \bar{\mu}^{(s)} \equiv \bar{\mu}(a_s) \tag{6.29}$$

where the areas per molecule in the discoidal, cylindrical and spherical parts of a micelle, a_d, a_c and a_s, are given by Eqs. (4.10) and (4.14).

At a given composition of the micelles, the dependence $\bar{\mu} = \bar{\mu}(a)$ is expected to have a minimum [42], as sketched in Fig. 4. At smaller a, the intermolecular repulsion prevails, whereas at larger a, the increased contact area between the micelle hydrophobic core with the surrounding water gives rise to an effective attraction.

At this point, we have to note that the fits of experimental data for $\bar{n}_M$ vs. X for disclike micelles with the general model from Sections 6.1–6.4 give values of the parameter $p = (\bar{\mu}^{(c)} - \bar{\mu}^{(d)})/(kT)$, which are positive, but close to zero (see Sections 8 and 9). In view of Eq. (6.29), this implies $\bar{\mu}(a_c) \approx \bar{\mu}(a_d)$. However, a_c is considerably greater than a_d, for example $a_c = 2a_d$; see Eq. (4.10). In such a case, the relation $\bar{\mu}(a_c) \approx \bar{\mu}(a_d)$ can be fulfilled only if a_c and a_d are located on the two sides of the minimum of the function $\bar{\mu}(a)$, as sketched in Fig. 4. The three possible cases, (i) $\bar{\mu}^{(c)} < \bar{\mu}^{(d)}$, i.e. $p < 0$ (Fig. 4a); (ii) $\bar{\mu}^{(c)} = \bar{\mu}^{(d)}$, i.e. $p = 0$ (Fig. 4b), and (iii) $\bar{\mu}^{(c)} > \bar{\mu}^{(d)}$, i.e. $p > 0$ (Fig. 4c), are discussed in Section 6.6 in relation to the free energy of the micellar solutions.

What concerns the chemical potential of a monomer in the *toroidal periphery* of a disclike micelle, $\bar{\mu}^{(t)} \equiv \bar{\mu}(a_t)$, for all configurations in Fig. 4 we have $\bar{\mu}^{(c)} \leqslant \bar{\mu}^{(t)} \leqslant \bar{\mu}^{(s)}$, insofar as $a_c \leqslant a_t \leqslant a_s$, see Eq. (4.13) and Fig. 4a. As mentioned above, the estimate of the derivative in Eq. (6.3) is equivalent to a linear interpolation of the $\bar{\mu}(a)$ dependence in the interval $a_c \leqslant a \leqslant a_s$.

6.6. Gibbs free energy of the micellar solution

It is convenient to scale the expression for the Gibbs free energy, $G = \sum_i N_i \mu_i$, with the number of water molecules, N_w:

$$g = \mu_w + X_1\mu_1 + \sum_{n=n_s}^{\infty} X_n\mu_n \tag{6.30}$$

Here, $g = G/N_w$ and μ_w is the chemical potential of water; for simplicity, we are working with a single-component surfactant. After
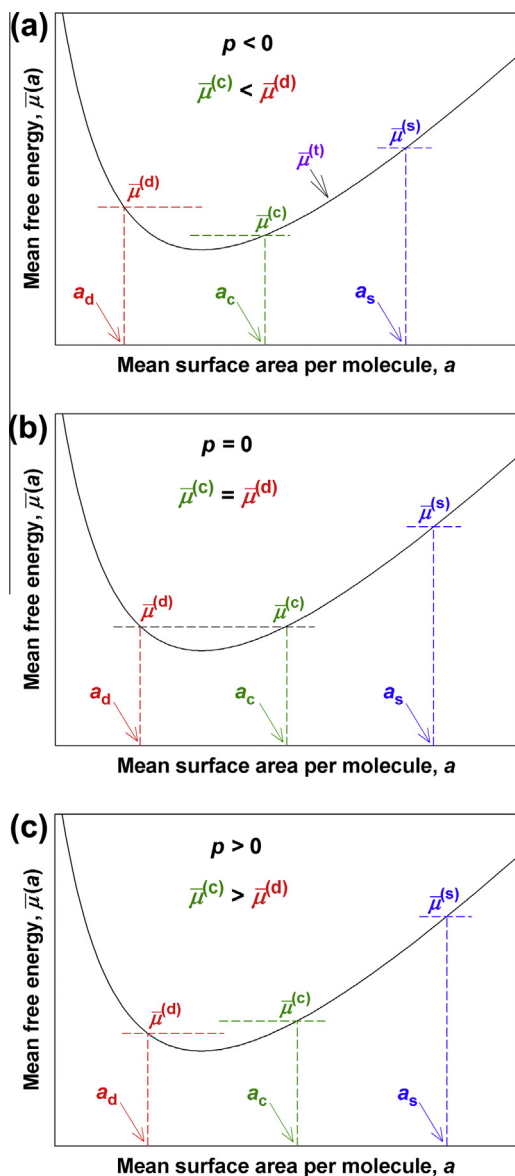
Fig. 4. Illustrative plot of the mean free energy $\bar{\mu}$ vs. the mean surface are per surfactant molecule in the micelle, a, for three different values of the parameter $p = (\bar{\mu}^{(c)} - \bar{\mu}^{(d)})/(kT)$: (a) $p < 0$; (b) $p = 0$; (c) $p > 0$; details in the text.

some transformations described in Appendix A.6, Eq. (6.30) acquires the form:

$$g = \tilde{\mu}_w - kT\left(X_1 + \sum_{n=n_s}^{\infty} X_n\right) + (\bar{\mu}^{(j)} - \varepsilon\, kT)X, \quad j = c, d \qquad (6.31)$$

As usual, the indices 'c' and 'd' denote cylindrical and disclike micelles.

Next, let us consider a solution with a given fixed total surfactant molar fraction X. The surfactant will self-assemble into disclike or cylindrical micelles depending on the sign of the quantity:

$$\Delta g \equiv g^{(c)} - g^{(d)} \qquad (6.32)$$

For $\Delta g > 0$ disclike micelles will form, whereas for $\Delta g < 0$ cylindrical micelles would appear. In view of the definition of p, Eq. (6.9), from Eqs. (6.31) and (6.32) we obtain:

$$\frac{\Delta g}{kT} = -X_1^{(c)} + X_1^{(d)} - \sum_{n=n_s}^{\infty}\left(X_n^{(c)} - X_n^{(d)}\right) + (p - \varepsilon^{(c)} + \varepsilon^{(d)})X \qquad (6.33)$$

By additional transformations, described in Appendix A.6, we derive:

$$\frac{\Delta g}{kT} \approx \sum_{n=n_s}^{\infty} X_n^{(d)} - \sum_{n=n_s}^{\infty} X_n^{(c)} + (p - \varepsilon^{(c)} + \varepsilon^{(d)})(X - X_1^{(c)}) \qquad (6.34)$$

At a given X, $\varepsilon^{(d)}$ is calculated by solving Eq. (6.15) numerically for the respective p value. $\varepsilon^{(c)}$ is calculated in the same way by setting $p = 0$. The sum with $X_n^{(d)}$ is calculated from Eq. (6.20) for the respective $\varepsilon^{(d)}$ and p. The sum with $X_n^{(c)}$ is calculated from Eq. (6.20) for the respective $\varepsilon^{(c)}$ and $p = 0$. In the calculations, one should take into account that $K^{(d)} = K^{(c)} \exp(pn_s)$.

Finally, Δg is calculated from Eq. (6.34).

The fact that $X_n^{(d)}\big|_{p=0} = X_n^{(c)}$, see Eq. (6.10), leads to $\Delta g = 0$ at $p = 0$. To see what is the behavior of Δg in the vicinity of the point $p = 0$, we carried out calculations using typical parameter values: $n_s = 83$, $\ln K = 35$ and $X_1^{(c)} \approx CMC = 1.44 \times 10^{-6}$ (see Section 8). The plot in Fig. 5 is almost linear, which means that the energy term with p in Eq. (6.34) is predominant, whereas the mixing-entropy terms, expressed by the sums in Eq. (6.34), give a relatively small contribution.

The results in Fig. 5 show that for $p < 0$ we have $\Delta g < 0$, i.e. the formation of disclike micelles is energetically unfavorable at negative p values, at which the surfactant forms cylindrical micelles. In contrast, at $p > 0$ we have $\Delta g > 0$, and disclike micelles should form.

At $p = 0$, the free energies of formation of disclike and cylindrical micelles are identical. Moreover, setting $\bar{\mu}^{(d)} = \bar{\mu}^{(c)}$ in Eq. (6.6) and $p = 0$ in Eq. (6.10), we obtain that in this case the micelle size distributions with respect to the aggregation number n are identical for cylindrical and disclike micelles. For this reason, at $p = 0$ Eqs. (2.16) and (2.19) give the same $\bar{n}_N$ and $\bar{n}_M$ for disclike and cylindrical micelles, and Eqs. (2.18) and (2.21) hold. One could discriminate between these two different micellar shapes from the experimental R_g and R_h values (Section 5), and from the measured viscosity (Section 8.6).

7. Disclike micelles: size limitations and numerical results

7.1. Limitations on the size of disclike micelles

The analysis in Section 6.6 indicates that for $p < 0$ the formation of disclike micelles is energetically disadvantageous, so that cylindrical micelles are formed in that case. Here, we will consider in more details the case $p > 0$, which corresponds to $\bar{\mu}^{(d)} < \bar{\mu}^{(c)}$ (Fig. 4c) and to the formation of *disclike* micelles. At positive p, we have $F(x)|_{\varepsilon=0} = -\pi p_s x$ in Eq. (6.12). Then, the integrals J_0, J_1
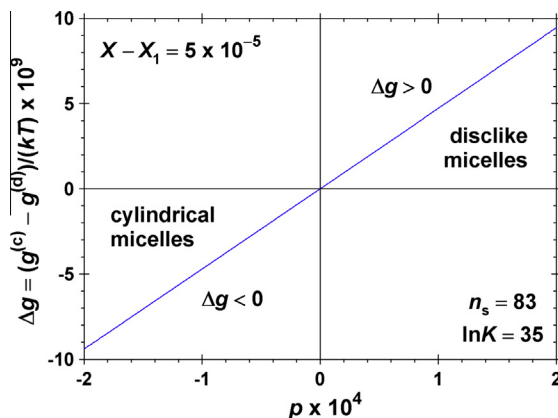
Fig. 5. Plot of Δg vs. p at a fixed total surfactant concentration, characterized by $X - X_1$, and at fixed n_s and $\ln K$. The regions with $\Delta g < 0$ and $\Delta g > 0$ correspond to the formation of cylindrical and disclike micelles, respectively.

and J_2 in Eqs. (6.21), (6.16), and (6.25) are *convergent* for $\varepsilon_s \to 0$. The maximal values of the respective integrals, which are attained at $\varepsilon_s = 0$, are:

$$J_{0,\max} = \frac{2}{\pi^2\, p_s^2} + \frac{1}{p_s} \tag{7.1}$$

$$J_{1,\max} = \frac{12}{\pi^4 p_s^4} + \frac{6}{\pi^2 p_s^3} + \frac{16 + 3\pi^2}{3\pi^2 p_s^2} + \frac{8}{3 p_s} \tag{7.2}$$

$$J_{2,\max} = \frac{240}{\pi^6 p_s^6} + \frac{120}{\pi^4 p_s^5} + \frac{64 + 24\pi^2}{\pi^4 p_s^4} + \frac{32 + 2\pi^2}{\pi^2 p_s^3} + \frac{128 + 48\pi^2}{9\pi^2 p_s^2}$$
$$+ \frac{64}{9 p_s} \tag{7.3}$$

Setting $\varepsilon_s \to 0$ in Eq. (6.15), we obtain the maximum value of X, denoted $X_{\max}$:

$$X_{\max} = X_1 + \frac{1}{K}\left(\frac{3n_s}{8}\right)^2\left(\frac{32}{9n_s} + J_{1,\max}\right) \tag{7.4}$$

where $J_{1,\max}$ is given by Eq. (7.2). From a physical viewpoint, this result means that for $p_s > 0$, disclike micelles can be formed only in a *limited range* of surfactant concentrations, viz. $X_1 < X \leqslant X_{\max}$. For a given p (for a given system), at $X = X_{\max}$, the micelle mean aggregation numbers $\bar{n}_N$ and $\bar{n}_M$ attain their maximal values, $\bar{n}_{N,\max}$ and $\bar{n}_{M,\max}$. These values can be obtained by replacing J_0, J_1 and J_2 in Eqs. (6.23) and (6.27) with their maximal values given by Eqs. (7.1)–(7.3).

7.2. Numerical results and discussion

To illustrate the dependence of $X_{\max}$ on p, in Fig. 6a we have plotted $X_{\max} - X_1$ vs. p calculated from Eq. (7.4) at typical parameter values, $n_s = 83$ and $\ln K = 35$ (see Section 8). Figs. 6b,c show the corresponding plots of the mass average aggregation number $\bar{n}_{M,\max}$ vs. p and of the micelle diameter ($L_{\max} + 2R$) vs. p. In particular, $L_{\max}$ is estimated as the positive root of the quadratic equation

$$\frac{\pi}{2} R L_{\max}^2 + \frac{\pi^2}{2} R^2 L_{\max} + \frac{4}{3}\pi R^3 = \bar{v}\, \bar{n}_{M,\max} \tag{7.5}$$

The left-hand side of Eq. (7.5) is the volume of the hydrophobic core of a toro-disc shaped micelle, $V_d + V_t$; see Eqs. (4.7) and (4.8); R and $\bar{v}$ are, respectively, the mean radius and volume per surfactant tail in the hydrophobic core of the micelle; see Eq. (4.2). In the calculations, we used typical values: $R = 2.04$ nm and $\bar{v} = 0.425$ nm³ (see Section 8).

The results shown in Fig. 6a are important for the understanding of the specificity of the growth of disclike micelles. Such micelles could exist only in the region confined between the two axes of the coordinate system and the theoretical curve $X_{\max} - X_1$ vs. p. In this region, at small p and large X the surfactant can form a relatively concentrated dispersion of large disclike micelles, so that eventually nematic or smectic phases from such micelles could appear [5,14,31]. In the region $p < 0$ cylindrical micelles are formed (see above).

At $X > X_{\max}$ (Fig. 6a) the formation of large lamellae is expected [1,31]. Indeed, at $p > 0$ the lower chemical potential of a molecule in the discoidal part of a micelle, $\bar{\mu}^{(d)} < \bar{\mu}^{(c)}$, favors the growth of *lamellar* structures. A theoretical analysis based on Ising Hamiltonians has also predicted that the size of disclike aggregates should jump from small to infinite [33,34]. In Fig. 6a, this should happen when crossing the boundary line $X_{\max} - X_1$ vs. p.

Fig. 6b shows a plot of $\bar{n}_{M,\max}$ vs. p at $n_s = 83$. (Note that this plot is independent of K.) One sees that large disclike aggregates (with $\bar{n}_M > 10 n_s$) could form only at $p < 0.01$. At $p < 3 \times 10^{-4}$, $\bar{n}_M$ could
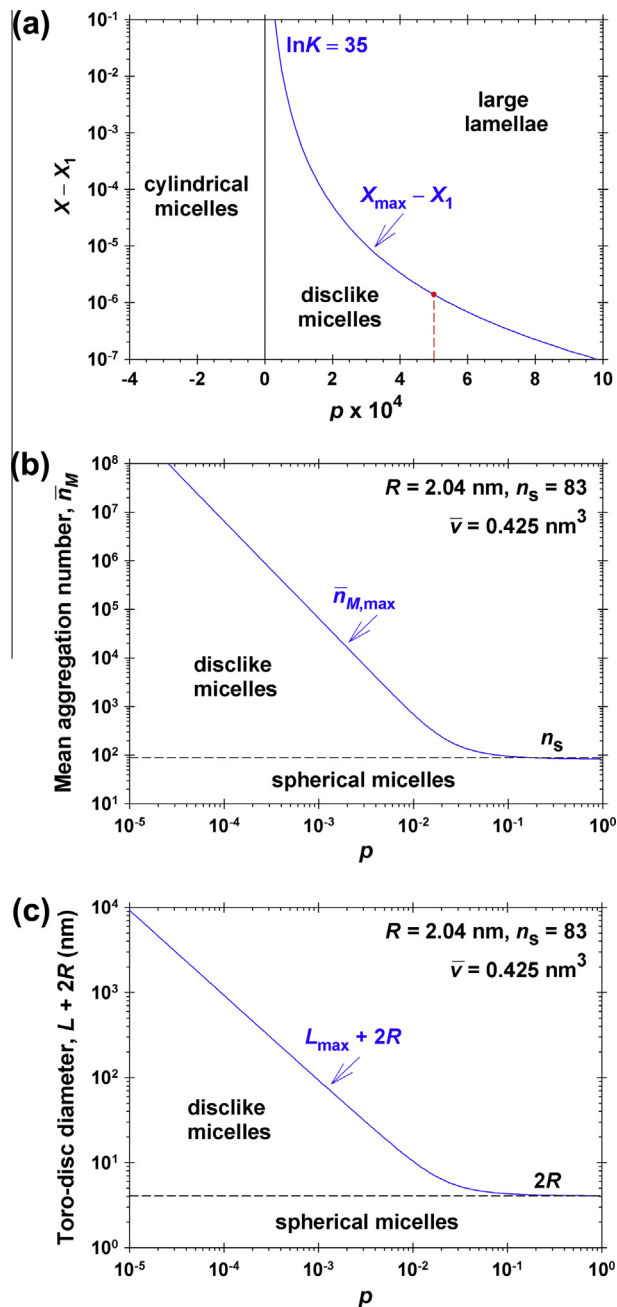
Fig. 6. (a) Plot of $X_{\max} - X_1$ vs. p calculated from Eq. (7.4); the phase domains with different micelles are shown. (b) Plot of $\bar{n}_M$ vs. p calculated from Eqs. (6.27), (7.2), and (7.3). (c) Plot of the toro-disc diameter with $L_{\max}$ calculated from Eq. (7.5) using the $\bar{n}_M$ values.

exceed 10^6. In contrast, at $p > 0.1$ we have $\bar{n}_{M,\max} \approx n_s$, i.e. the disclike micelles are transformed into spherical ones. The limited range of p values, $0 < p < 0.1$, where disclike micelles can form (Fig. 6b) explains why they represent a rare form of self-assembly as compared to the cylindrical ones.

Fig. 6c shows the corresponding plot of $L_{\max} + 2R$ vs. p calculated for typical parameter values denoted in the figure. One sees that the mean diameter of the disclike micelles could exceed 1 μm at $p < 10^{-4}$. In contract, at $p > 0.1$ the disc diameter is $\approx 2R$, i.e. the micelles are almost spherical.

Note that for $0 < p < 0.01$, the theoretical dependencies in Figs. 6b,c are practically linear in double log scale. Indeed, from Eq. (6.27), along with Eqs. (7.2), (7.3), (7.4), (7.5), it follows that

the leading terms of the series expansions of the respective quantities at $p \ll 1$ are:

$$\bar{n}_{M,max} \approx \frac{160}{3\pi^2 n_s} \frac{1}{p^2}; \quad L_{max} \approx \left(\frac{320\bar{v}}{3\pi^3 n_s R}\right)^{1/2} \frac{1}{p};$$

$$X_{max} - X_1 = \frac{256}{3\pi^4 K n_s^2} \frac{1}{p^4} \qquad (7.6)$$

The limitations on the growth of disclike micelles, related to the existence of maximal values, such as X_{max}, $\bar{n}_{M,max}$ and L_{max}, call for discussion. These maximal values appear because at $p > 0$ all integrals in Section 6 are convergent for $\varepsilon \to 0$. (In contrast, for $p \leqslant 0$ all these integrals diverge at $\varepsilon \to 0$, which corresponds to the growth of increasingly large micelles with the rise of surfactant concentration.) The convergence of the integrals at $p > 0$ is due to the term with p in Eq. (6.10), which takes into account the increment of the excess peripheral energy of the disclike micelle. Thus, disclike micelles could appear only at $p > 0$ (Fig. 5), but the positive p leads to a rise of the micelle peripheral energy with the increase of the disc diameter, which in turns limits the micelle growth (Fig. 6).

The upward motion along the vertical dashed line in Fig. 6a corresponds to increase of the surfactant molar fraction, X, in a given system (at a fixed p). With the increase of X, the parameter ε decreases, until reaching $\varepsilon = 0$ at $X = X_{max}$, i.e. at the boundary line of the region with disclike micelles. A negative value of ε would lead to divergence of all integrals in Section 6, which means that the considered model is not applicable for $\varepsilon < 0$.

Fig. 7 shows the variation of $\bar{n}_M$ with the rise of surfactant concentration (characterized by X) for a given system, which corresponds to a fixed p value. The lower line is identical for cylindrical micelles and for disclike micelles with $p = 0$; see the discussion in the last paragraph of Section 6.6. The mean aggregation number $\bar{n}_M$ increases with the rise of both $X - X_1$ and p. At fixed p, each curve $\bar{n}_M$ vs. $X - X_1$ has an end-point of coordinates $(X_{max} - X_1, \bar{n}_{M,max})$ that can be determined from Figs. 6a,b for the respective p. The upper dash-dotted line consists of all these end-points.

The line with $p = 0$ is described by the dependence $\bar{n}_M \approx 2[K(X - X_1)]^{1/2}$ following from Eq. (2.21). In addition, by eliminating p between the first and third formula in Eq. (7.6) we obtain:

$$\bar{n}_{M,max} \approx \frac{10}{\sqrt{3}}[K(X_{max} - X_1)]^{1/2} \qquad (7.7)$$

Hence, in a double-log scale the dependences of both $\bar{n}_M|_{p=0}$ and $\bar{n}_{M,max}$ on $X - X_1$ are parallel straight lines of slope 1/2; see Fig. 7.
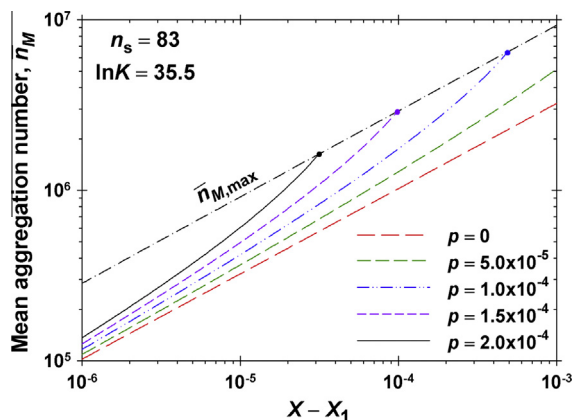
The region with disclike micelles, confined between these to lines, appears as a relatively narrow band of width characterized by the ratio $\bar{n}_{M,max}/\bar{n}_M|_{p=0} \approx 5/\sqrt{3} \approx 2.89$.

8. Test of the model against data for mixed micelles

8.1. Experimental system and results

As mentioned above, in Ref. [14] it was established that the addition of lauric acid to a mixed micellar solution leads to the appearance of disclike micelles in a given range of concentrations of the three surfactants. The investigated solutions contained 11 wt% SDS and 3 wt% cocamidopropyl betaine (CAPB). The concentration of lauric acid was varied between 0 and 3.5 wt%.

We carried out experiments with a similar system. The zwitterionic surfactant was CAPB product of Goldschmidt GmbH with commercial name Tego® Betain F50. By electrolytic conductivity measurements, it was established that 100 mM CAPB contain 112 mM NaCl as an admixture. The anionic surfactant was sodium laurylethersulfate with one ethylene-oxide group (SLES-1EO), product of Stepan Co. This surfactant will be denoted SLES for brevity. The used lauric (dodecanoic) acid (LA), $\geqslant$99.5%, was a product of Acros Organics. In all experiments the molar ratio CAPB/SLES was constant, 4:1. The temperature was 25 °C. The micelle growth in mixed CAPB + SLES solutions in the absence of LA was studied in Ref. [51].

The viscosity of the micellar solutions was measured by a programmable viscometer DV-II + Pro (Brookfield, USA). For diluted micellar solutions, static and dynamic light scattering (SLS and DLS) experiments were carried out with a Malvern 4700C (Malvern Instruments, UK) goniometric light scattering system with a solid state laser (532 nm).

Fig. 8 shows a plot of the measured viscosity of solutions containing 80 mM CAPB and 20 mM SLES vs. the concentration of added lauric acid. The viscosity exhibits a high and sharp maximum (peak) between 11 and 15 mM lauric acid. Because the peak is observed only in the narrow vicinity of a certain fatty acid concentration, the phenomenon looks like a resonance rise of viscosity.

The observed effect (Fig. 8) is stronger than that in Ref. [14], insofar as the peak in viscosity is higher (598 vs. 175 mPa s) and is observed at a lower surfactant concentration (100 vs. 480 mM). The main differences between the two experimental systems are that here the anionic surfactant is SLES, rather than SDS, and that the molar ratio zwitterionic/anionic surfactant here is 80:20 CAPB/SLES vs. 20:80 CAPB/SDS in Ref. [14].

Fig. 7. Plots of the mass average aggregation umber, $\bar{n}_M$, vs. $X - X_1$ calculated from Eqs. (6.15) and (6.27) for different systems corresponding to different fixed p values. The upper dash-dotted curve, representing the set of the end-points of the $\bar{n}_M$ curves, is calculated from Eqs. (6.27), (7.2)–(7.4); see the text for details.
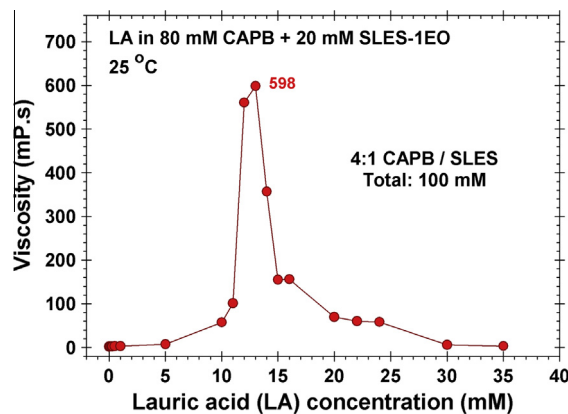

Fig. 8. Plot of the solution's viscosity vs. the concentration of lauric acid added to 4:1 CAPB/SLES micellar solutions at a fixed 100 mM (3.51 wt%) total concentration of CAPB + SLES.

Note that the growth of both rodlike and disclike micelles leads to a rise of the solution's viscosity, the minimal being the viscosity of spherical micelles at the same volume fraction [52,53].

Our goal here is to demonstrate how the developed theoretical model compares with light-scattering data for disclike micelles. For this reason, we carried out SLS and DLS experiments with *diluted* micellar solutions of viscosity close to that of water. The dilution was necessary to avoid interactions between the formed micelles. (The investigation of the *concentrated* solutions of high viscosity will be a subject of a subsequent experimental study.)

The concentrated stock solution (which was subjected to dilution) contained 80 mM CAPB + 20 mM SLES-1EO + 10 mM lauric acid. This solution had viscosity $\eta = 57$ mPa s corresponding to the region just before the maximum (with $\eta_{max} = 598$ mPa s) in Fig. 8. The stock solution was diluted with 110 mM NaCl aqueous solution (with the same ionic strength as of the stock solution) and the prepared samples were left to equilibrate for at least 24 h at 25 °C. The obtained experimental values of the hydrodynamic and gyration radii, R_h and R_g, determined by DLS and SLS, respectively, at various total CAPB + SLES concentrations, c_{tot}, are given in Table 1.

8.2. Determining the micelle shape from the light scattering data

The simplest way to establish whether the micelles are disclike or cylindrical is to analyze the data for R_h and R_g by using the models of oblate and prolate spheroid, as described below.

For an *oblate spheroid* (Fig. 9), R_h obeys the following relationship [50]:

$$\sqrt{a^2/b^2 - 1} = \tan\left(\sqrt{a^2 - b^2}/R_h\right) \tag{8.1}$$

where a is the semi-major axis and b is the semi-minor axis.

For $b = 2.8$ nm (estimated as the length of the CAPB molecule) and for each experimental R_h, Eq. (8.1) is solved numerically to determine a. The computations show that only the first root of Eq. (8.1) (where the tangent's argument is between 0 and $\pi/2$) has physical meaning. The obtained value of a is used to calculate R_g from the expression [50]:

$$R_g = \left(\frac{2a^2 + b^2}{5}\right)^{1/2} \quad \text{(oblate spheroid)} \tag{8.2}$$

The values of R_g calculated in this way from the experimental R_h are given in the fourth column of Table 1.

In the alternative case of *prolate spheroid* (prolate ellipsoid of revolution), R_h obeys the following relationship [50]:

$$R_h \ln\left(\frac{a}{b} + \sqrt{a^2/b^2 - 1}\right) = \sqrt{a^2 - b^2} \tag{8.3}$$

As before, a is the semi-major axis and b is the semi-minor axis, but this time of the prolate spheroid.
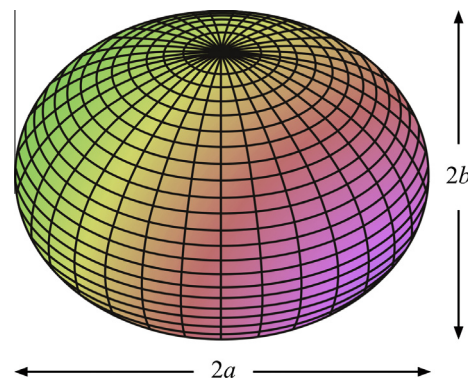

Fig. 9. Oblate spheroid (oblate ellipsoid of revolution) with semi-major axis a and semi-minor axis b.

For $b = 2.8$ nm and for each experimental R_h from Table 1, a is determined by numerically solving Eq. (8.3), which has a single positive root. Next, R_g is calculated by substituting the obtained a in the equation [50]:

$$R_g = \left(\frac{a^2 + 2b^2}{5}\right)^{1/2} \quad \text{(prolate spheroid)} \tag{8.4}$$

The values of R_g calculated in this way from the experimental R_h are given in the sixth column of Table 1.

The data in Table 1 show that the experimental values of R_g are close to the R_g values calculated from the oblate spheroid model, but they are very different from R_g calculated using the prolate spheroid model. Consequently, in this experiment we are dealing with disclike, rater than cylindrical micelles.

8.3. Determination of X_1, n_s and some geometrical parameters

The total molar fraction of the surfactant monomers of all kinds can be estimated as $X_1 \approx v_w \times CMC$, where $v_w \approx 30 \times 10^{-30}$ m^3 is the volume per water molecule in the solution at room temperature and CMC is the critical micellization concentration of the mixed surfactant solution (here, expressed in number of molecules per m^3). For the investigated mixed micelles of CAPB, SLES and lauric acid in molar ratio 80:20:10, the CMC can be estimated from the formula [54]:

$$\frac{110}{CMC} = \frac{80}{0.088} + \frac{20}{0.1} + \frac{10}{0.04} \Rightarrow CMC = 0.08 \text{ mM} \tag{8.5}$$

where 0.088 and 0.1 mM are the CMCs of CAPB and the used SLES, whereas 0.04 mM is the average solubilization constant of lauric acid in CAPB and SLES micelles [55].

The mean aggregation number of the spherical micelles, n_s, can be estimated by geometric considerations, using the Tanford formulas for the length, l, and volume, v, of the surfactant hydrocarbon tail [42]:

Table 1
Comparison of the experimental R_g with the respective values of R_g calculated from the experimental R_h using the models of oblate and prolate spheroid.

c_{tot} (mM)	Experiment		Oblate spheroid model		Prolate spheroid model	
	R_h (nm)	R_g (nm)	R_g (nm)	ΔR_g[a] (nm)	R_g (nm)	ΔR_g[a] (nm)
0.20	51.9 ± 1.6	49.9	50.5	1.6	122.5	4.7
0.25	54.5 ± 1.7	50.2	53.0	1.7	130.1	5.0
0.30	62.2 ± 1.9	52.1	60.7	1.9	153.0	5.7
0.40	67.6 ± 1.1	52.3	66.0	1.1	169.3	3.4
0.50	70.5 ± 2.6	52.3	68.9	2.6	178.2	8.0

[a] ΔR_g is the error of the calculated R_g corresponding to the experimental error of R_h.

$$l = (0.154 + 0.1265 n_C) \text{ nm} \tag{8.6}$$

$$v = (27.4 + 26.9 n_C) \times 10^{-3} \text{ nm}^3 \tag{8.7}$$

where n_C is the number of carbon atoms in a saturated hydrocarbon chain. Thus we obtain:

$$l_1 = 2.18, \quad l_2 = l_3 = 1.67 \text{ (nm)} \tag{8.8}$$

$$v_1 = 0.458, \quad v_2 = 0.350, v_3 = 0.323 \text{ (nm}^3) \tag{8.9}$$

The subscripts 1, 2 and 3 refer to CAPB, SLES and lauric acid. Then, from Eqs. (4.1) and (4.2) we determine:

$$R = 2.04 \text{ nm}, \quad \bar{v} = 0.425 \text{ nm}^3, \quad n_s = 83 \tag{8.10}$$

In addition, from Eqs. (4.1) and (4.10) we find:

$$a_d = 0.21, \quad a_c = 0.42, \quad a_s = 0.63 \text{ (nm}^2) \tag{8.11}$$

For comparison, the headgroup cross-sectional areas of the investigated three surfactants are

$$a_{h,1} = 0.28, \quad a_{h,2} = 0.43, \quad a_{h,3} = 0.23 \text{ (nm}^2) \tag{8.12}$$

For $a_{h,1}$ and $a_{h,3}$, see Refs. [56,57]; $a_{h,2}$ is estimated in the same way as in Ref. [56] by fit of surface tension isotherm for SLES from Ref. [58].

The area per molecule in the discoidal part of a micelles, estimated as $a_d = \bar{v}/R = 0.21$ nm^2 is smaller than the area per headgroup of the lauric acid, $a_{h,3} = 0.23$ nm^2. For this reason, a_d has to be estimated from Eqs. (4.14) and (4.15) using the parameter values in Eq. (8.12). The result reads $a_d = a_h = 0.30$ nm^2. The latter value is smaller than a_c and considerably smaller than a_s, see Eq. (8.11).

The hydrodynamic radius of a spherical micelle can be estimated as $b = R + 0.76 = 2.8$ nm, where $\delta_h = 0.76$ nm is the length of the headgroup of the predominant component, CAPB.

8.4. Determination of the mass average aggregation number $\bar{n}_M$

The mass average aggregation number can be estimated by division of the total volume of the micelle hydrophobic core, V_{core}, on the mean volume per hydrocarbon tail, $\bar{v}$:

$$\bar{n}_M = \frac{V_{core}}{\bar{v}} \tag{8.13}$$

see e.g. Ref. [44]. For determining V_{core}, different geometric models are possible. For example, one can use the model of *oblate spheroid* (Fig. 9) and to determine its major semi-axis, a, from the experimental R_h at known b by using Eq. (8.1); see above. Then, the volume of the oblate spheroid is:

$$V_{core} = \frac{4}{3}\pi(a - \delta_h)^2(b - \delta_h) \text{ (oblate spheroid)} \tag{8.14}$$

δ_h is the average diameter of a surfactant headgroup.

Alternatively, one can model the disclike micelle as a *toro-disc* (Fig. 3) and to determine $V_{core} = V_d + V_t$ from Eqs. (4.7) and (4.8):

$$V_{core} = \frac{\pi}{2}RL^2 + \frac{\pi^2}{2}R^2 L + \frac{4}{3}\pi R^3 \text{ (toro-disc)} \tag{8.15}$$

where $L = 8(R_h - b)/3$, see Eq. (5.5).

Using the data in Table 1, for each R_h we calculated $\bar{n}_M$ for oblate spheroid and toro-disc from Eqs. (8.13), (8.14), (8.15). Table 2 contains the obtained $\bar{n}_M$ values, as well as the semi-major axis of the oblate spheroid, a, which is compared with the analogous parameter, $L/2 + b$, for the toro-disc. The same value of $b = 2.8$ nm (the length of the CAPB molecule) is used for oblate spheroid and toro-disc. The calculated V_{core} for oblate spheroid is systematically smaller, but not so different from V_{core} for toro-disc. The semi-axis

a of the oblate spheroid is markedly longer than $L/2 + b$. This is understandable, because at the same maximal thickness b, the average thickness of the oblate spheroid is smaller than that of the toro-disc, which is compensated by an increase in the length of the major semi-axis a to get the same R_h.

8.5. Determination of the parameters p and K

The used procedure for data processing is as follows:

(1) A tentative value is assigned to p_s.
(2) For each experimental value of $\bar{n}_M$ for toro-disc (Table 2), we calculate ε_s by solving numerically Eq. (6.27).
(3) The obtained ε_s is substituted in Eqs. (6.15), and $K(X - X_1)$ is calculated using also Eqs. (6.17) and (6.18).
(4) The obtained $K(X - X_1)$ values, corresponding to different experimental $\bar{n}_M$, are plotted vs. the experimental $X - X_1$; see Fig. 10a.
(5) The parameter p_s is varied until the plot of the calculated $K(X - X_1)$ vs. the experimental $X - X_1$ complies with a linear regression of zero intercept; see the solid line in Fig. 10a. This regression determines the physical value of p_s, and its slope gives the physical value of K.

The points in Fig. 10a represent data from the first and last columns of Table 2, recalculated in terms of $(X - X_1)$ and $K(X - X_1)$ by using the above procedure. (Note that c_{tot} in Table 2 includes only CAPB and SLES, but the concentration of lauric acid is also included in the values of $X - X_1$ plotted along the horizontal axis.) The best fit, given by the solid line in Fig. 10a, corresponds to $p_s = 0.001$ and $\ln K = 35.2$. For $n_s = 83$, in view of Eq. (6.6) we calculate $(\bar{\mu}^{(s)} - \bar{\mu}^{(d)})/(kT) = (\ln K)/n_s = 0.42$, which is a reasonable value. In addition, from Eqs. (6.9) and (6.13) we obtain:

$$p \equiv \frac{\bar{\mu}^{(c)} - \bar{\mu}^{(d)}}{kT} = \frac{8p_s}{3n_s} = 3.2 \times 10^{-5} \tag{8.16}$$

In spite of being small, the above value of p is accurately determined, because small variations in p_s produce a significant effect on the fit, as illustrated in Fig. 10a.

As mentioned above, the physical value of p_s corresponds to the linear regression that has a zero intercept (Fig. 10a). Because the intercept of this plot is sensitive to X_1, the value of X_1 (i.e. of the CMC) is essential for the present procedure of data processing, despite the relation $X_1 \ll X$.

In Fig. 10b, the data for $\bar{n}_M$ (Table 2, toro-disc) are plotted vs. $(X - X_1)^{1/2}$. The solid line corresponds to the theoretical fit at $p_s = 0.001$ from Fig. 10a. The dashed line is a fit of the experimental points in Fig. 10b with a linear regression of zero intercept in accordance with the equation $\bar{n}_M \approx 2[K(X - X_1)]^{1/2}$. The latter dependence corresponds to $p_s = 0$. Because of the small value of p_s for the theoretical fit, the two lines in Fig. 10b almost coincide. In particular, the slope of the linear regression yields $\ln K = 35.3$, which is close to $\ln K = 35.2$ determined from the theoretical fit in Fig. 10a. In other words, the value of K can be obtained with a good accuracy by a linear regression fit as in Fig. 10b. However, the value of p_s can be determined only by using the full procedure illustrated in Fig. 10a.

8.6. Discussion on the predictions of the model

Here, we discuss the predictions of the model regarding the transition from disclike to cylindrical micelles. At $p \to 0$ the distribution of the disclike micelles by aggregation number, Eq. (6.10), is gradually transformed into the respective distribution for cylindrical micelles. In other words, $\bar{n}_M$ does not exhibit any jump when

Table 2
Geometrical parameters of disclike micelles and their mean aggregation number $\bar{n}_M$ calculated by using the models of oblate spheroid and toro-disc.

Experiment		Oblate spheroid			Toro-disc		
c_{tot} (mM)	R_h (nm)	a (nm)	V_{core} (nm³)	$\bar{n}_M$ Eq. (8.13)	$L/2 + b$ (nm)	V_{core} (nm³)	$\bar{n}_M$ Eq. (8.13)
0.20	51.9	79.8	52,284	123,022	68.3	57,561	135,422
0.25	54.5	83.8	57,713	135,796	71.7	63,666	149,783
0.30	62.2	95.9	75,767	178,275	82.0	83,548	196,558
0.40	67.6	104	89,916	211,568	89.2	99,101	233,148
0.50	70.5	109	98,078	230,773	93.1	108,001	254,087
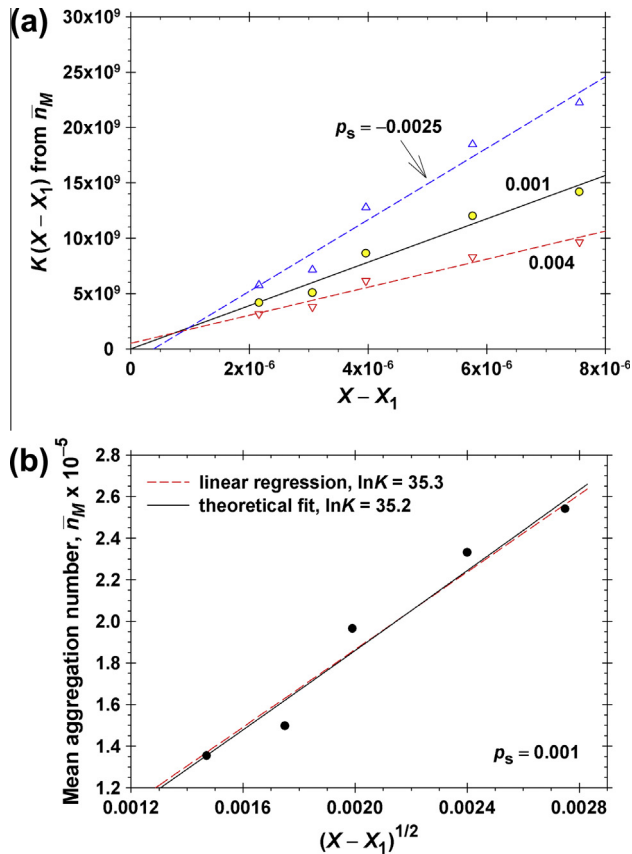
Fig. 10. (a) Plot of experimental data from Table 2 as $K(X - X_1)$ vs. $X - X_1$, where $K(X - X_1)$ is calculated from the experimental $\bar{n}_M$ using Eqs. (6.15) and (6.27), whereas $X - X_1$ is determined from c_{tot}. The three sets of data correspond to three p_s values shown in the figure. The lines are fits of the respective data by linear regression. The best fit is that of zero intercept, which corresponds to $p_s = 0.001$ and $\ln K = 35.2$. (b) Plot of $\bar{n}_M$ vs. $(X - X_1)^{1/2}$; the points are data from Table 2 for toro-disc; the solid line corresponds to the theoretical fit at $p_s = 0.001$; the dashed line is the fit of the data points by linear regression with zero intercept.
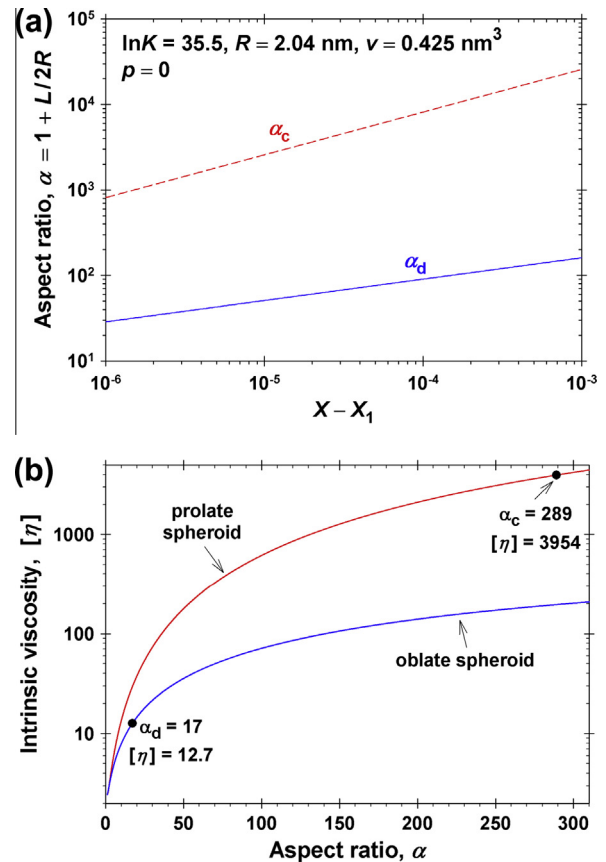

Fig. 11. (a) Plot of the aspect ratio, α, vs. the surfactant concentration characterized by $X - X_1$, at typical values of the parameters K, R, and v, and for $p = 0$; α_c and α_d are calculated using the sphero-cylinder and toro-disc models, respectively. (b) Plot of tabulated data from Ref. [59] for the intrinsic viscosity $[\eta]$ vs. the aspect ratio, α, for prolate and oblate spheroids. It is illustrated that the transformation of disclike micelles with $\alpha_d = 17$ into cylindrical ones corresponds to a jump from the point (17, 12.7) to the point (289, 3954); see Eq. (8.19).

crossing the border between the disclike and cylindrical micelles in Fig. 6a. However, at the same $\bar{n}_M$ the viscosity undergoes a jump, because of a huge change in the *aspect ratio*, α, upon a transition from disclike to cylindrical micelles, or vice versa.

To demonstrate that, let us consider an oblate and a prolate spheroid of the same volume V (corresponding to the same $\bar{n}_M$). For the oblate spheroid we have:

$$V = \frac{4}{3}\pi a^2 b \Rightarrow \alpha_d \equiv \frac{a}{b} = \left(\frac{3V}{4\pi b^3}\right)^{1/2} \qquad (8.17)$$

where α_d is the aspect ratio for the oblate spheroid that models a disclike micelle. Likewise, for the prolate spheroid we obtain:

$$V = \frac{4}{3}\pi a b^2 \Rightarrow \alpha_c \equiv \frac{a}{b} = \frac{3V}{4\pi b^3} \qquad (8.18)$$

where α_c is the aspect ratio for the prolate spheroid modeling a cylindrical micelle. The comparison of Eqs. (8.17) and (8.18) shows that

$$\alpha_c = \alpha_d^2 \qquad (8.19)$$

In Fig. 11a, we have plotted α_c and α_d vs. the surfactant concentration characterized by $X - X_1$. The lower line of the plot of $\bar{n}_M$ vs. $X - X_1$ in Fig. 7 with $p = 0$ has been used. The $\bar{n}_M$ values have been transformed into L values using the approach from Section 8.4. α_c has been estimated for a sphero-cylinder, whereas α_d – for a toro-disc of the same volume (the same aggregation number). One sees that α_c is between 28 and 160 times greater than α_d in the considered concentration range.

In Fig. 11b, we have plotted the dependence of the intrinsic viscosity, $[\eta]$, on the aspect ratio, α, for low shear rates, as tabulated by Scheraga [59] for oblate and prolate spheroids. As an example, it is shown that if disclike micelles of aspect ratio $\alpha_d = 17$ are transformed into cylindrical micelles of aspect ratio $\alpha_c = \alpha_d^2 = 289$, see Eq. (8.19), then the intrinsic viscosity $[\eta]$ would jump from 12.7 to 3954, i.e. 311 times.

In non-diluted micellar solutions, in which the interactions between the aggregates upon shearing are not negligible, the viscosity can be described by the Krieger–Dougherty formula [53,60]:

$$\frac{\eta}{\eta_0} = \left(1 - \frac{\phi}{\phi_{max}}\right)^{-[\eta]\phi_{max}} \tag{8.20}$$

where ϕ is the volume fraction of the micelles considered as solid particles, whereas ϕ_{max} is the maximum possible value of ϕ, at which the viscosity η diverges. Note that $[\eta]$ appears as an exponent in Eq. (8.20), and its jump upon transitions from disclike to cylindrical micelles must be accompanied by a significant change in the solution's viscosity.

For the experimental system 80:20 CAPB/SLES + LA investigated in the present section, we determined a rather small value, $p = 3.2 \times 10^{-5}$, for the disclike micelles. In other words, the investigated system is very close to the border between the domains with disclike and cylindrical micelles at $p = 0$ (Fig. 6a). Then, it is possible the addition of lauric acid to cause a small variation in $\bar{\mu}^{(c)} - \bar{\mu}^{(d)}$ that leads to $p \leqslant 0$ in a certain interval of LA concentrations. In this interval, the disclike micelles would transform into cylindrical ones, which would cause a high peak in the solution's viscosity. This could be one possible explanation of the peak in Fig. 8, which will be verified in a subsequent experimental study at high surfactant concentrations and viscosities. In the present study, we focus on the comparison between theory and experiment (DLS and SLS) in the case of relatively diluted micellar solutions of viscosity close to that of pure water; see Table 1 and Section 9.

9. Test of the model against data for disclike micelles from fluorinated surfactants

We tested the model also against light-scattering data for R_h and R_g of fluorinated surfactants from Ref. [7]. The surfactants are N-(1,1-dihydroperfluorooctyl)-N,N,N-trimethylammonium chloride [$C_7F_{15}CH_2N^+(CH_3)_3Cl^-$] and N-(1,1-dihydroperfluorododecyl)-N,N,N-trimethyl-ammonium chloride [$C_{11}F_{23}CH_2N^+(CH_3)_3Cl^-$]. Hereafter, for brevity they will be denoted as C8-TAC and C12-TAC, respectively. As demonstrated in Ref. [7], the investigated solutions of these surfactants contain disclike micelles. From the values of R_h, we estimated L, V_{core} and $\bar{n}_M$ following the same approach as in Section 8.3 using the toro-disc model. The results are summarized in Table 3. Details on the procedure of calculations, including the estimate of n_s, can be found in Appendix A.7.

As seen in Table 3, the disclike micelles from the surfactant with longer hydrophobic tail, C12-TAC, have significantly greater aggregation numbers, $\bar{n}_M$, than the C8-TAC micelles. Further, from the values of $\bar{n}_M$ in Table 3, using the procedure illustrated in Fig. 10a, we determined the values of the parameters p_s and K, which are listed in Table 4.

The values of p in Table 4 are smaller than 0.01 and belong to the region of large disclike micelles; see Fig. 6b. For C12-TAC, the values of p and $\ln K$ are close to those for the mixed micelles considered in Section 8, which also have hydrophobic chains with 12 carbon atoms. The relatively large value of $\mu^{(s)} - \mu^{(d)} = 1.51\ kT$ for C8-TAC is understandable, because for such a short-tail surfactant the spherical micelles have a low aggregation number n_s with a

Table 3
Geometrical parameters of disclike micelles from fluorinated C8-TAC and C12-TAC and their mean aggregation numbers calculated by using the toro-disc model.

c_{tot} (mM)	R_h (nm)*	R_g (nm)*	L (nm)	V_{core} (nm³)	$\bar{n}_M$
C8-TAC (CMC = 13.6 mM)[a]					
54.4	23	35	56	6205	14,775
68.0	26	33	64	8028	19,115
109	32	35	80	12,377	29,470
C12-TAC (CMC = 0.25 mM)[a]					
2.25	97	135	252	171,162	283,381
3.00	106	139	276	204,900	339,238
3.75	110	125	287	220,868	365,675

[a] The values of R_h, R_g, and the CMC are from Ref. [7].
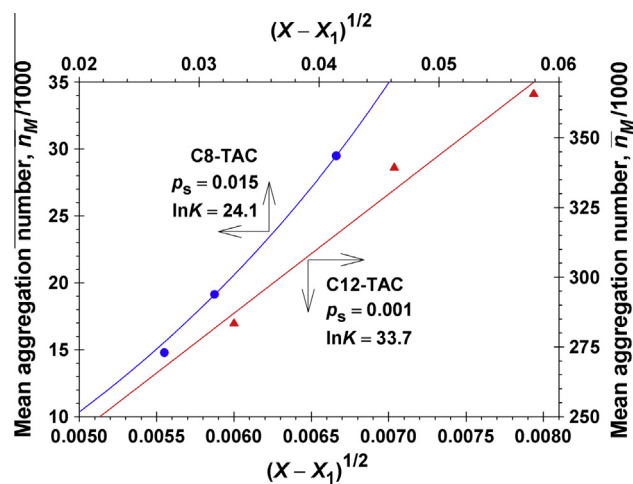
Table 4
Parameters of the disclike micelles from fluorinated C8-TAC and C12-TAC determined from the experimental $\bar{n}_M$ vs. X dependence using the theoretical model.

Parameter	C8-TAC	C12-TAC
n_s	16	33
p_s	0.015	0.001
$\ln K$	24.1	33.7
$p = (\mu^{(c)} - \mu^{(d)})/(kT)$	2.5×10^{-3}	8.1×10^{-5}
$(\mu^{(s)} - \mu^{(d)})/(kT)$	1.51	1.02

large area of contact between water and the hydrophobic zones among the headgroups, which leads to a rise of $\mu^{(s)}$.

Fig. 12 shows the data for $\bar{n}_M$ vs. $(X - X_1)^{1/2}$ for C8-TAC and C12-TAC from Table 3, as well as the respective theoretical dependences calculated from Eqs. (6.15) and (6.27) with the parameter values in Table 4. The theory agrees with the experiment. For C12-TAC the value of p is small, and for this reason the theoretical curve is close to a straight line. However, for C8-TAC the theoretical dependence is markedly curved because of the greater value of p. We recall that the linear asymptotic dependence $\bar{n}_M \approx 2[K(X - X_1)]^{1/2}$ holds for $p = 0$, and it can be satisfied also for small p values ($p < 10^{-4}$).

Finally, it is worthwhile noting that the $\bar{n}_M$ vs. $(X - X_1)^{1/2}$ plot of SANS data for cesium perfluorooctanoate in Ref. [6] also complies with a straight line, which means that the disclike micelles detected in this study are characterized with a small value of p, as discussed above.

Fig. 12. Plot of data for $\bar{n}_M$ vs. $(X - X_1)^{1/2}$ for C8-TAC and C12-TAC from Table 3; the solid lines are the respective theoretical dependences calculated from Eqs. (6.15) and (6.27) with the parameter values in Table 4.

10. Conclusions

Here, expanding the ladder model by Missel et al. [41], we developed a detailed theoretical model describing the growth of disclike surfactant micelles. Theoretical expressions are derived for the concentration dependences of the number and mass average aggregation numbers of toro-disc shaped micelles, $\bar{n}_N$ and $\bar{n}_M$. The theory shows that the growth of disclike micelles is governed by the difference between the standard chemical potentials of a surfactant molecule in disclike and cylindrical micelles, characterized by the parameter $p = (\bar{\mu}^{(c)} - \bar{\mu}^{(d)})/kT$. For $p < 0$, the formation of disclike micelles is energetically disadvantageous, and the surfactant forms cylindrical micelles. In contrast, for $p > 0$, disclike micelles are formed. However, $p > 0$ corresponds to positive excess peripheral energy of the micelles, which increases with the rise of their diameters. For this reason, disclike micelles can appear in a restricted concentration range and for small peripheral energies, $0 < p < 0.1$.

Because of the small values of the parameter p, the problem for its determination by analysis of experimental data is rather non-trivial. The conventional plot of $\bar{n}_M$ vs. $(X - X_1)^{1/2}$ [6,41,43–45] cannot be used for this purpose. In Section 8.5, we propose a new procedure for data analysis, which allows determination of the two basic parameters of the model, p and K, with a good accuracy from light-scattering data.

The procedure was applied to interpret data for the concentration dependence of hydrodynamic radius R_h for disclike micelles. Three sets of light-scattering data for different surfactants were processed, using the derived original expressions for R_g and R_h for toro-disc shaped micelles, Eqs. (5.3) and (5.5). It is remarkable that in all cases the best fit gives $p \ll 0.1$, in agreement with the theoretical predictions. It is possible to have such small p values because the dependence of the surfactant chemical potential on the area per headgroup at the micelle surface exhibits a minimum [42], so that $\bar{\mu}^{(d)}$ and $\bar{\mu}^{(c)}$ are situated at almost the same level on the two sides of this minimum (see Fig. 4). This role of the minimum in the $\bar{\mu}(a)$ curve for the transitions between disclike and cylindrical micelles is established for the first time in the present study.

The driving force for the growth of disclike micelles is the lower value of $\bar{\mu}^{(d)}$ relative to $\bar{\mu}^{(c)}$, which leads to a gain of free energy upon the transfer of each surfactant molecule into the *central discoidal part* of the micelle at $p > 0$. The positive *peripheral energy* of the disclike micelle opposes the micelle growth preventing the formation of micelles bigger than a given maximal size at a given p (see Section 7). Moreover, at $p > 0$ the positive excess peripheral energy preserves the round shape of the micelles. In contrast, if a sufficiently large disclike micelle occasionally forms at $p < 0$, its peripheral energy would be negative, which would give rise to a branching instability [61].

In addition, at $p \to 0$ the model predicts a transition from disclike to cylindrical micelles, which occurs at the *same* size distribution, and consequently, at the same mean aggregation number, $\bar{n}_M$, and mean volume. Under such conditions, the micelle aspect ratio and viscosity undergo a significant jump-wise increase (Section 8.6). One of the potential applications of the model is to provide an explanation of experimentally observed peaks in viscosity; see e.g. Fig. 8.

In general, the model can be used for analyzing the shape and size of micelles in various surfactant solutions. In particular, the indication for the formation of discoidal aggregates only in the special case $0 < p < 0.1$ shows why disclike micelles are observed much less frequently than cylindrical ones, as noted in preceding studies [1,2]. Further extensions of the model are possible for ribbon-like (tablet-shaped) micelles [39], as well as for mixed disclike aggregates where the central and peripheral parts of the micelles have different compositions [2,24].

Appendix A. Supplementary material

Supplementary data associated with this article can be found, in the online version, at http://dx.doi.org/10.1016/j.jcis.2013.11.002.

References

[1] T. Zemb, M. Dubios, B. Deme, T. Guli-Kryzywicki, Science 283 (1999) 816–819.
[2] Y. Song, R.M. Dorin, R.M. Garcia, Y.-B. Jiang, H. Wang, P. Li, Y. Qiu, F. van Swol, J.E. Miller, J.A. Shelnutt, J. Am. Chem. Soc. 130 (2008) 12602–12603.
[3] T. Rades, C.C. Müller-Goymann, Int. J. Pharm. 159 (1997) 215–222.
[4] D. Danino, Curr. Opin. Colloid Interface Sci. 17 (2012) 316–329.
[5] M.C. Holmes, D.J. Reynolds, N. Boden, J. Phys. Chem. 91 (1987) 5257–5262.
[6] H. Iijima, T. Kato, H. Yoshida, M. Imai, J. Phys. Chem. B 102 (1998) 990–995.
[7] K. Matsuoka, A. Yonekawa, M. Ishii, C. Honda, K. Endo, Y. Moroi, Y. Abe, T. Tamura, Colloid Polym. Sci. 285 (2006) 323–330.
[8] K. Matsuoka, M. Ishii, A. Yonekawa, C. Honda, K. Endo, Y. Moroi, Y. Abe, T. Tamura, Bull. Chem. Soc. Jpn. 80 (2007) 1129–1131.
[9] J. Eastoe, P. Rogueda, D. Shariatmadari, R. Heenan, Colloids Surf., A 117 (1996) 215–225.
[10] H.-T. Jung, S.Y. Lee, E.W. Kaler, B. Coldren, J.A. Zasadzinski, PNAS 99 (2002) 15318–15322.
[11] J. Hao, H. Hoffmann, Curr. Opin. Colloid Interface Sci. 9 (2004) 279–293.
[12] D. Carrière, L. Belloni, B. Demé, M. Dubois, C. Vautrin, A. Meister, T. Zemb, Soft Matter 5 (2009) 4983–4990.
[13] E. Blanco, U. Olsson, J.M. Ruso, P.C. Schulz, G. Prieto, F. Sarmiento, J. Colloid Interface Sci. 331 (2009) 522–531.
[14] G. Colafemmina, R. Recchia, A.S. Ferrante, S. Amin, G. Palazzo, J. Phys. Chem. B 114 (2010) 7250–7260.
[15] J. Wu, E.M. Pearce, T.K. Kwei, A.A. Lefebvre, N.P. Balsara, Macromolecules 35 (2002) 1791–1796.
[16] W.F. Edmonds, Z. Li, M.A. Hillmyer, T.P. Lodge, Macromolecules 39 (2006) 4526–4530.
[17] H. Cui, Z. Chen, K.L. Wooley, D.J. Pochan, Macromolecules 39 (2006) 6599–6607.
[18] H. Cui, Z. Chen, S. Zhong, K.L. Wooley, D.J. Pochan, Science 317 (2007) 647–650.
[19] L. Yin, M.A. Hillmyer, Macromolecules 44 (2011) 3021–3028.
[20] S.J. Holder, N.A.J.M. Sommerdijk, Polym. Chem. 2 (2011) 1018–1028.
[21] H. Kawamura, Y. Murata, T. Yamaguchi, H. Igimi, M. Tanaka, G. Sugihara, J.P. Kratohvil, J. Phys. Chem. 93 (1989) 3321–3326.
[22] D.M. Small, Adv. Chem. Ser. B 84 (1968) 31–52.
[23] D. Madenci, S.U. Egelhaaf, Curr. Opin. Colloid Interface Sci. 15 (2010) 109–115.
[24] N.A. Mazer, G.B. Benedek, M.C. Carey, Biochemistry 19 (1980) 601–615.
[25] P.K. Vinson, J.R. Bellare, H.T. Davis, W.G. Miller, L.E. Scriven, J. Colloid Interface Sci. 42 (1991) 74–91.
[26] C.R. Sanders, G.C. Landis, Biochemistry 34 (1995) 4030–4040.
[27] E. Johansson, M.C. Sandström, M. Bergström, K. Edwards, Langmuir 24 (2008) 1731–1739.
[28] J. Leng, S.U. Egelhaaf, M.E. Cates, Europhys. Lett. 59 (2002) 311–317.
[29] M. Johnsson, K. Edwards, Biophys. J. 85 (2003) 3839–3847.
[30] B. Donnio, Curr. Opin. Colloid Interface Sci. 7 (2002) 371–394.
[31] M.S. Leaver, M.C. Holmes, J. Phys. II France 3 (1993) 105–120.
[32] A. Nesrullajev, Mater. Chem. Phys. 123 (2010) 546–550.
[33] R. Granek, W.M. Gelbart, Y. Bohbot, A. Ben-Shaul, J. Chem. Phys. 101 (1994) 4331–4342.
[34] W.M. Gelbart, A. Ben-Shaul, J. Phys. Chem. 100 (1996) 13169–13189.
[35] J.A. Cuesta, R.P. Sear, Eur. Phys. J. B 8 (1999) 233–243.
[36] B. Halle, M. Landgren, B. Jönsson, J. Phys. France 49 (1988) 1235–1259.
[37] A.G. Daful, J.B. Avalos, A.D. Mackie, Langmuir 28 (2012) 3730–3743.
[38] M.M. Kozlov, D. Lichtenberg, D. Andelman, J. Phys. Chem. B 101 (1997) 6600–6606.
[39] L.M. Bergström, S. Skoglund, K. Danerlöv, V.M. Garamus, J.S. Pedersen, Soft Matter 7 (2011) 10935–10944.
[40] J.N. Israelachvili, D.J. Mitchell, B.W. Ninham, J. Chem. Soc., Faraday Trans. I (72) (1976) 1525–1568.
[41] P.J. Missel, N.A. Mazer, G.B. Benedek, C.Y. Young, M.C. Carey, J. Phys. Chem. 84 (1980) 1044–1057.
[42] J.N. Israelachvili, Intermolecular and Surface Forces, Academic Press, London, 2011.

[43] R.G. Alargova, V.P. Ivanova, P.A. Kralchevsky, A. Mehreteab, G. Broze, Colloids Surf., A 142 (1998) 201–218.
[44] R.G. Alargova, K.D. Danov, P.A. Kralchevsky, G. Broze, A. Mehreteab, Langmuir 14 (1998) 4036–4049.
[45] R.G. Alargova, J.T. Petkov, D.N. Petsev, J. Colloid Interface Sci. 261 (2003) 1–11.
[46] P. Mukerjee, J. Phys. Chem. 76 (1972) 565–570.
[47] T. Kennedy, Discrete Comput. Geom. 35 (2006) 255–267.
[48] C.M. Sorensen, D. Shi, Opt. Commun. 178 (2000) 31–36.
[49] B.J. Berne, R. Pecora, Dynamic Light Scattering, Wiley, New York, 2000.
[50] W. Van de Sande, A. Persoons, J. Phys. Chem. 89 (1985) 404–406.
[51] N.C. Christov, N.D. Denkov, P.A. Kralchevsky, K.P. Ananthapadmanabhan, A. Lips, Langmuir 20 (2004) 565–571.
[52] E.J. Hinch, L.G. Leal, J. Fluid Mech. 52 (1972) 683–712.
[53] T.M. Kwon, M.S. Jhon, H.J. Choi, J. Mol. Liq. 75 (1998) 115–126.
[54] K.D. Danov, P.A. Kralchevsky, K.P. Ananthapadmanabhan, Adv. Colloid Interface Sci. (2013), http://dx.doi.org/10.1016/j.cis.2013.02.001.
[55] S.S. Tzocheva, P.A. Kralchevsky, K.D. Danov, G.S. Georgieva, A.J. Post, K.P. Ananthapadmanabhan, J. Colloid Interface Sci. 369 (2012) 274–286.
[56] K.D. Danov, S.D. Kralchevska, P.A. Kralchevsky, K.P. Ananthapadmanabhan, A. Lips, Langmuir 20 (2004) 5445–5453.
[57] K.D. Danov, P.A. Kralchevsky, K.P. Ananthapadmanabhan, A. Lips, J. Colloid Interface Sci. 300 (2006) 809–813.
[58] D. Vollhardt, G. Czichocki, R. Rudert, Colloids Surf., A 142 (1998) 315–322.
[59] H.A. Scheraga, J. Chem. Phys. 23 (1955) 1526–1532.
[60] I.M. Krieger, T.J. Dougherty, Trans. Soc. Rheol. 3 (1959) 137–152.
[61] M. Tang, W.C. Carter, J. Phys. Chem. B 117 (2013) 2898–2905.

Appendix A. Supplementary material

This Appendix contains the mathematical derivations of some equations
and estimates of some parameters used in the article:

Disclike vs. cylindrical micelles: generalized model of micelle growth and data interpretation

by S.E. Anachkov, P.A. Kralchevsky, K.D. Danov, G.S. Georgieva,
and K.P. Ananthapadmanabhan

(The cited references can be found in the reference list of the main article, with the same numbers)

Appendix A.1. Volume and surface area of a toro-disc shaped micelle

Let us consider a toro-disc of thickness $2R$, which coincides with the curvature radius of the semitoroidal periphery, and with diameter L of the central discoidal part; see Fig. 2 in the main article. Let us choose the plane $z = 0$ of the cylindrical coordinate system, Orz, to coincide with the midplane of the toro-disc; r is the radial coordinate. The volume V of the toro-disc is a sum of the volume of the disc, V_d, and that of the semitorus, V_t:

$$V = V_d + V_t \tag{A.1}$$

$$V_d = \frac{\pi}{2} R L^2 \tag{A.2}$$

The volume of the semitorus, V_t, is given by the integral:

$$V_t = 4\pi \int_0^R dz \int_{L/2}^{L/2+\sqrt{R^2-z^2}} r\,dr = 2\pi \int_0^b [(\frac{L}{2} + \sqrt{R^2 - z^2})^2 - \frac{L^2}{4}]\,dz$$

$$= 2\pi \int_0^R (L\sqrt{R^2 - z^2} + R^2 - z^2)\,dz = 2\pi L R^2 \int_0^1 \sqrt{1 - \tilde{z}^2}\,d\tilde{z} + \frac{4\pi}{3} R^3 = \frac{\pi^2}{2} R^2 L + \frac{4\pi}{3} R^3$$

that is

$$V_t = \frac{\pi^2}{2} R^2 L + \frac{4\pi}{3} R^3 \tag{A.3}$$

The surface area A of the toro-disc is a sum of the area of the two disc surfaces, A_d, plus the surface area of the semitorus, A_t:

1

$$A = A_d + A_t \tag{A.4}$$

$$A_d = \frac{\pi}{2}L^2 \tag{A.5}$$

The surface area of the semitorus, A_t, is given by the integral:

$$A_t = 4\pi \int_{L/2}^{L/2+R} [1+(\frac{\mathrm{d}z_t}{\mathrm{d}r})^2]^{1/2} r\,\mathrm{d}r$$

where $z_t(r)$ is the equation of the generatrix of the upper surface of the semitorus:

$$z_t = [R^2 - (r - \frac{L}{2})^2]^{1/2} \quad \text{and} \quad \frac{\mathrm{d}z_t}{\mathrm{d}r} = -\frac{r - L/2}{[R^2 - (r - L/2)^2]^{1/2}}$$

Thus, we obtain:

$$A_t = 4\pi R \int_{L/2}^{L/2+R} \frac{r}{[R^2 - (r - L/2)^2]^{1/2}}\,\mathrm{d}r = 4\pi R \int_0^R \frac{\tilde{r} + L/2}{(R^2 - \tilde{r}^2)^{1/2}}\,\mathrm{d}\tilde{r}$$

$$= 4\pi R \int_0^{\pi/2} (R\sin t + \frac{L}{2})\,\mathrm{d}t = \pi^2 RL + 4\pi R^2$$

that is

$$A_t = \pi^2 RL + 4\pi R^2 \tag{A.6}$$

Eqs. (A.3) and (A.6) correspond to Eq. (4.8) in the main text of the article.

Appendix A.2. Radius of gyration of a toro-disc shaped micelle

The squared radius of gyration, R_g^2, is the second moment of the mass distribution of a given body, scaled with its total mass [48]. For a body of uniform mass density, R_g^2 is given by the expression:

$$R_g^2 = \frac{1}{V}\int_V |\mathbf{r}|^2\,\mathrm{d}V \tag{A.7}$$

The origin of the position vector $\mathbf{r}$ is in the mass center of the body of volume V; $\mathrm{d}V$ is the volume element. In the considered case of *toro-disc* (see Fig. 3 in the main article), we have:

$$\int_V |\mathbf{r}|^2 \, \mathrm{d}V = 4\pi \int_0^b \mathrm{d}z \int_0^{L/2+\sqrt{b^2-z^2}} (r^2 + z^2) r \, \mathrm{d}r = 4\pi \int_0^b [\frac{(L/2+\sqrt{b^2-z^2})^4}{4} + \frac{(L/2+\sqrt{b^2-z^2})^2}{2} z^2] \mathrm{d}z$$

$$= \pi b \int_0^{\pi/2} [(\frac{L}{2} + b\cos t)^4 + 2(\frac{L}{2} + b\cos t)^2 b^2 \sin^2 t] \cos t \, \mathrm{d}t$$

Taking the last integral, we obtain:

$$\int_V |\mathbf{r}|^2 \, \mathrm{d}V = \frac{\pi}{16} b L^4 (1 + 2\pi \frac{b}{L} + \frac{56}{3}\frac{b^2}{L^2} + 8\pi \frac{b^3}{L^3} + \frac{64}{5}\frac{b^4}{L^4})$$

Expressing V from Eqs. (A.1)–(A.3), with R replaced by b, we finally derive:

$$R_g^2 = \frac{L^2}{8} \frac{1 + 2\pi \dfrac{b}{L} + \dfrac{56}{3}\dfrac{b^2}{L^2} + 8\pi \dfrac{b^3}{L^3} + \dfrac{64}{5}\dfrac{b^4}{L^4}}{1 + \pi \dfrac{b}{L} + \dfrac{8b^2}{3L^2}}$$

The last equation is identical to Eq. (5.3) in the main text of the article.

Appendix A.3. Hydrodynamic radius of a toro-disc shaped micelle

In dynamic light scattering, the hydrodynamic radius, R_h, of a particle is determined from the experimentally determined average translational diffusion coefficient using the Stokes-Einstein formula. For a body of uniform density, R_h can be estimated from the expression [24]:

$$\frac{1}{R_h} = \frac{2}{3V} \int_V \frac{1}{|\mathbf{r}|} \mathrm{d}V \tag{A.8}$$

The origin of the position vector $\mathbf{r}$ is in the mass center of the body of volume V; $\mathrm{d}V$ is the volume element. One could verify that for a spherical particle of radius R, Eq. (A.8) yields $R_h = R$. Moreover, for oblate and prolate spheroids the integration in Eq. (A.8) leads to Eqs. (8.1) and (8.3) in the main text.

In the considered case of *toro-disc* (see Fig. 3 in the main article), we obtain:

$$\int_V \frac{1}{|\mathbf{r}|} \mathrm{d}V = 4\pi \int_0^b \mathrm{d}z \int_0^{L/2+\sqrt{b^2-z^2}} \frac{r}{\sqrt{r^2 + z^2}} \mathrm{d}r = 4\pi \int_0^b [\sqrt{(\frac{L}{2} + \sqrt{b^2-z^2})^2 + z^2} - z] \mathrm{d}z$$

$$= 4\pi \int_0^b (\sqrt{\frac{L^2}{4} + b^2 + L\sqrt{b^2-z^2}} - z) \mathrm{d}z = 4\pi b^2 \int_0^{\pi/2} [(1 + \frac{L^2}{4b^2} + \frac{L}{b}\cos t)^{1/2} - \sin t] \cos t \, \mathrm{d}t$$

Hence, R_h can be expressed in the form:

$$R_{\mathrm{h}} = \frac{b}{J_{\mathrm{h}}}, \tag{A.9}$$

$$J_{\mathrm{h}} \equiv \frac{2}{1 + \dfrac{3\pi}{8}\dfrac{L}{b} + \dfrac{3}{8}\dfrac{L^2}{b^2}} \int\limits_0^{\pi/2} [(1 + \frac{L^2}{4b^2} + \frac{L}{b}\cos t)^{1/2} - \sin t]\cos t\, \mathrm{d}t \tag{A.10}$$

The last integral cannot be solved analytically. Asymptotic expansions can be found for small and large L/b. Thus, in the case of $L/b \ll 1$, the series expansion in Eq. (A.10) yields:

$$R_{\mathrm{h}} = b(1 + \frac{\pi}{8}\frac{L}{b} - \frac{3\pi^2 - 28}{96}\frac{L^2}{b^2} + ...) \quad \text{for} \quad L \ll b \tag{A.11}$$

In the opposite case of $L/b \gg 1$, the asymptotic expansion in Eq. (A.10) leads to:

$$R_{\mathrm{h}} = \frac{3L}{8}(1 + \frac{\pi+2}{2}\frac{b}{L} + \frac{12-\pi^2}{4}\frac{b^2}{L^2} + ...) \quad \text{for} \quad L \gg b \tag{A.12}$$

For $L/b \to 0$, Eq. (A.11) yields $R_{\mathrm{h}} = b$, whereas for $b/L \to 0$, Eq. (A.12) reduces to $R_{\mathrm{h}} = 3L/8$. Combining the last two values, we obtain an approximate expression, which turns out to be rather accurate for all L/b values:

$$R_{\mathrm{h}} \approx b + \frac{3}{8}L \tag{A.13}$$

The accuracy of Eq. (A.13) is illustrated in Fig. A.1, where it is seen that the magnitude of the relative error of this approximate equation is smaller than 0.005 for all possible values of L/b.
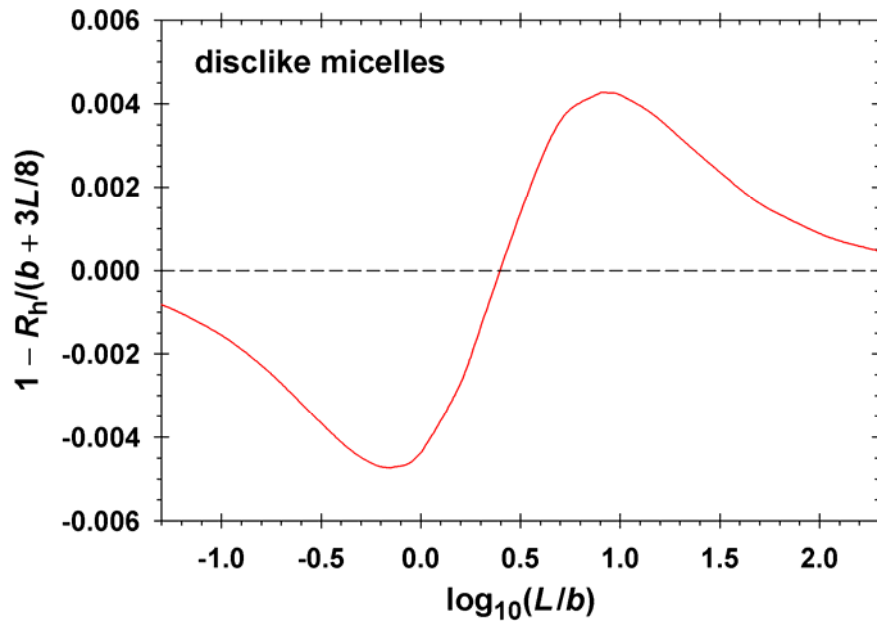
Fig. A.1. Relative error of the approximate Eq. (A.13) vs. $\log_{10}(L/b)$.

Appendix A.4

Expression for the mean chemical potential of a surfactant molecule in the micelles

Insofar as the disclike micelle is modeled as a combination of disc and torus, $\tilde{\mu}_n$ can be expressed in the form:

$$\tilde{\mu}_n = \overline{\mu}^{(d)}(n - n_t) + \overline{\mu}^{(t)} n_t \tag{A.14}$$

Here, n is the total aggregation number; n_t is the number of surfactant molecules in the toroidal periphery of the micelle; $\overline{\mu}^{(d)}$ and $\overline{\mu}^{(t)}$ are mean standard chemical potentials of a molecule that belongs to the discoidal and toroidal part of the micelle, respectively. In the case of cylindrical micelles, the spherical caps are independent of the micelle length, L, whereas for disclike micelles the area per molecule in the toroidal periphery, a_t, depends on L. To take into account the latter dependence, in Eq. (A.14) we expand $\overline{\mu}^{(t)}$ in series around $a = a_s$:

$$\tilde{\mu}_n = \overline{\mu}^{(d)}n + (\overline{\mu}^{(t)} - \overline{\mu}^{(d)})n_t \approx \overline{\mu}^{(d)}n + \left[\overline{\mu}^{(s)} + \left.\frac{\partial\overline{\mu}}{\partial a}\right|_{a=a_s}(a_t - a_s) - \overline{\mu}^{(d)}\right]n_t$$

$$= \overline{\mu}^{(d)}n + \left.\frac{\partial\overline{\mu}}{\partial a}\right|_{a=a_s}(a_t - a_s)n_t + (\overline{\mu}^{(s)} - \overline{\mu}^{(d)})(n_t - n_s) + (\overline{\mu}^{(s)} - \overline{\mu}^{(d)})n_s \tag{A.15}$$

With the help of Eqs. (4.1), (4.11) and (4.12) from the main article, we obtain:

$$(a_t - a_s)n_t = -\frac{\pi^2}{2}RL \tag{A.16}$$

Because $a_c \leq a_t \leq a_s$, the derivative in Eq. (A.15) can be estimated as follows:

$$\left.\frac{\partial\overline{\mu}}{\partial a}\right|_{a=a_s} \approx \frac{\overline{\mu}^{(s)} - \overline{\mu}^{(c)}}{a_s - a_c} = (\overline{\mu}^{(s)} - \overline{\mu}^{(c)})\frac{R}{\overline{v}} \tag{A.17}$$

where we have used the fact that $a_s - a_c = \overline{v}/R$; see Eq. (4.10) in the main article. The multiplication of Eqs. (A.16) and (A.17), leads to:

$$\left.\frac{\partial\overline{\mu}}{\partial a}\right|_{a=a_s}(a_t - a_s)n_t = -(\overline{\mu}^{(s)} - \overline{\mu}^{(c)})\frac{\pi^2 R^2 L}{2\overline{v}} \tag{A.18}$$

The subtraction of Eqs. (4.1) from Eq. (4.11) in the main article yields:

$$n_\mathrm{t} - n_\mathrm{s} = \frac{\pi^2 R^2 L}{2\bar{v}},$$ (A.19)

In view of Eqs. (A.19), the substitution of Eq. (A.18) in Eq. (A.15) leads to:

$$\tilde{\mu}_n \approx \bar{\mu}^{(\mathrm{d})} - (\bar{\mu}^{(\mathrm{d})} - \bar{\mu}^{(\mathrm{c})})\frac{3\pi L}{8R} n_\mathrm{s} + (\bar{\mu}^{(s)} - \bar{\mu}^{(\mathrm{d})})n_\mathrm{s}$$ (A.20)

where the two terms with $\bar{\mu}^{(\mathrm{s})}(n_\mathrm{t} - n_\mathrm{s})$ have cancelled each other. Finally, the subtraction of $n\bar{\mu}^{(1)}$ from Eq. (A.20) yields Eq. (6.4) in the main article.

Appendix A.5. Calculation of sums using integrals

Our starting point will be the identity:

$$\sum_{n=n_\mathrm{s}}^{\infty} f(n) = \frac{f(n_\mathrm{s})}{2} + \left[\frac{f(n_\mathrm{s}) + f(n_\mathrm{s}+1)}{2} + \frac{f(n_\mathrm{s}+1) + f(n_\mathrm{s}+2)}{2} + ...\right]\Delta n$$ (A.21)

where $\Delta n = 1$. The Euler-Maclaurin approximate formula reads:

$$\int_{n_\mathrm{s}}^{\infty} f(n)\,\mathrm{d}n \approx \frac{f(n_\mathrm{s}) + f(n_\mathrm{s}+1)}{2}\Delta n + \frac{f(n_\mathrm{s}+1) + f(n_\mathrm{s}+2)}{2}\Delta n + ...$$ (A.22)

The above formula is very accurate for every function $f(n)$ that varies slowly in the interval $[n, n+1]$ for $n_\mathrm{s} \le n < \infty$. Note that each term in the right-hand side of Eq. (A.22) represents the area of a trapezoid of height Δn. In other words, the integral is replaced with a sum of the areas of trapezoids. The combination of Eqs. (A.21) and (A.22) yields:

$$\sum_{n=n_\mathrm{s}}^{\infty} f(n) \approx \frac{f(n_\mathrm{s})}{2} + \int_{n_\mathrm{s}}^{\infty} f(n)\,\mathrm{d}n$$ (A.23)

To illustrate the validity and precision of Eq. (A.23) for the sums used in the present study, let us first consider a simple geometrical progression, like that in the denominator of Eq. (2.16) of the main article (case of cylindrical micelles):

$$f(n) = (1-\varepsilon)^n \quad \text{for} \quad 0 < \varepsilon \ll 1$$ (A.24)

The exact expression for the sum, and its series expansion read:

$$\sum_{n=n_s}^{\infty} f(n) = \frac{1}{\varepsilon}(1-\varepsilon)^{n_s} = \frac{1}{\varepsilon} - n_s + \frac{n_s(n_s-1)}{2}\varepsilon + \dots \tag{A.25}$$

For comparison, Eq. (A.23) gives the following result:

$$\frac{f(n_s)}{2} + \int_{n_s}^{\infty} f(n)\,\mathrm{d}n = \frac{1}{2}(1-\varepsilon)^{n_s} - \frac{(1-\varepsilon)^{n_s}}{\ln(1-\varepsilon)} = \frac{1}{\varepsilon} - n_s + [\frac{n_s(n_s-1)}{2} - \frac{1}{12}]\varepsilon + \dots \tag{A.26}$$

One sees that the first two terms in the expansions (A.25) and (A.26) coincide, and the third terms are also very close, because for typical micelles $n_s = 60 - 80$.

Another example is the sum that appears in the numerator of Eq. (2.16):

$$f(n) = n(1-\varepsilon)^n \quad \text{for} \quad 0 < \varepsilon << 1 \tag{A.27}$$

The exact expression for the above sum and its series expansion read:

$$\sum_{n=n_s}^{\infty} f(n) = (1-\varepsilon)^{n_s}(\frac{1}{\varepsilon^2} + \frac{n_s-1}{\varepsilon}) = \frac{1}{\varepsilon^2} - \frac{1}{\varepsilon} - \frac{n_s(n_s-1)}{2} + \dots \tag{A.28}$$

For comparison, Eq. (A.23) gives the following result:

$$\frac{f(n_s)}{2} + \int_{n_s}^{\infty} f(n)\,\mathrm{d}n = \frac{n_s}{2}(1-\varepsilon)^{n_s} + \frac{(1-\varepsilon)^{n_s}}{\ln^2(1-\varepsilon)}[1 - n_s\ln(1-\varepsilon)]$$

$$= \frac{1}{\varepsilon^2} - \frac{1}{\varepsilon} - \frac{n_s(n_s-1)}{2} + \frac{1}{12} + \dots \tag{A.29}$$

The comparison of Eqs. (A.28) and (A.29) show that again Eq. (A.23) works very accurately, with a minor difference (1/12) in the third term of the expansion in Eq. (A.29).

Finally, let us consider a sum that appears in the numerator of Eq. (2.19):

$$f(n) = n^2(1-\varepsilon)^n \quad \text{for} \quad 0 < \varepsilon << 1 \tag{A.30}$$

The exact expression for the above sum, and its series expansion read:

$$\sum_{n=n_s}^{\infty} f(n) = (1-\varepsilon)^{n_s}[\frac{2}{\varepsilon^3} + \frac{2n_s-3}{\varepsilon^2} + \frac{(n_s-1)^2}{\varepsilon}] = \frac{2}{\varepsilon^3} - \frac{3}{\varepsilon^2} + \frac{1}{\varepsilon} + \dots \tag{A.31}$$

Eq. (A.23) gives the following result:

$$\frac{f(n_s)}{2} + \int_{n_s}^{\infty} f(n)\,\mathrm{d}n = \frac{n_s^2}{2}(1-\varepsilon)^{n_s} - \frac{(1-\varepsilon)^{n_s}}{\ln^3(1-\varepsilon)}[2 - 2n_s\ln(1-\varepsilon) + n_s^2\ln^2(1-\varepsilon)]$$

$$= \frac{2}{\varepsilon^3} - \frac{3}{\varepsilon^2} + \frac{1}{\varepsilon} + \dots \tag{A.32}$$

In this case, Eq. (A.23) gives exactly the first three terms in the series expansion; compare Eqs. (A.31) and (A.32).

Appendix A.6. Calculation of the free energy of the micellar solution

It is convenient to scale the expression for the Gibbs free energy, $G = \sum_i N_i \mu_i$, with the number of water molecules, N_w:

$$g = \mu_w + X_1 \mu_1 + \sum_{n=n_s}^{\infty} X_n \mu_n \qquad (A.33)$$

Here, $g \equiv G/N_w$ and μ_w is the chemical potential of water; for simplicity, we are working with a single-component surfactant. Substituting the expressions for the chemical potentials of monomers and micelles, and eliminating $\ln X_n$ with the help of Eq. (2.2) in the main article, we bring Eq. (A.33) in the form:

$$g = \mu_w + X\tilde{\mu}_1 + XkT \ln X_1 \qquad (A.34)$$

where Eq. (2.9) has been used and the tilde denotes standard chemical potential. Further, using the definition $X_1/X_B = \exp(-\varepsilon)$, along with Eqs. (3.11) and (6.7) in the main text, we obtain:

$$\ln X_1 = -\varepsilon + (\overline{\mu}^{(j)} - \tilde{\mu}_1)/kT, \quad j = c, d \qquad (A.35)$$

As usual, the indices 'c' and 'd' denote cylindrical and disclike micelles. The chemical potential of the water molecules in the micellar solution is:

$$\mu_w = \tilde{\mu}_w + kT \ln(1 - X_1 - \sum_{n=n_s}^{\infty} X_n) \qquad (A.36)$$

Substituting Eqs. (A.35) and (A.36) into Eq. (A.34), we finally get:

$$g = \tilde{\mu}_w - kT(X_1 + \sum_{n=n_s}^{\infty} X_n) + (\overline{\mu}^{(j)} - \varepsilon kT)X \qquad (A.37)$$

where the leading term in the expansion of logarithm in Eq. (A.36) has been retained.

Now, let us consider a solution with a given fixed total surfactant molar fraction X. The surfactant will self-assemble into disclike or cylindrical micelles depending on the sign of the quantity:

$$\Delta g \equiv g^{(c)} - g^{(d)} \qquad (A.38)$$

For $\Delta g > 0$ disclike micelles will form, whereas for $\Delta g < 0$ cylindrical micelles will appear. In view of the definition of p, Eq. (6.9) in the main text, from Eqs. (A.37) and (A.38) we obtain:

$$\frac{\Delta g}{kT} = -X_1^{(c)} + X_1^{(d)} - \sum_{n=n_s}^{\infty}(X_n^{(c)} - X_n^{(d)}) + (p - \varepsilon^{(c)} + \varepsilon^{(d)})X \tag{A.39}$$

Using Eq. (6.7)–(6.9) in the main text, we derive:

$$
\begin{aligned}
X_1^{(d)} &= \exp[\frac{\overline{\mu}^{(c)} - \overline{\mu}^{(1)}}{kT} - p - \varepsilon^{(d)}] = X_B^{(c)}\exp[-p - \varepsilon^{(d)}] \\
&= X_1^{(c)}\exp[-p - \varepsilon^{(d)} + \varepsilon^{(c)}] \approx X_1^{(c)}(1 - p - \varepsilon^{(d)} + \varepsilon^{(c)})
\end{aligned}
\tag{A.40}
$$

The substitution of Eq. (A.40) into Eq. (A.39) finally yields:

$$\frac{\Delta g}{kT} \approx \sum_{n=n_s}^{\infty}X_n^{(d)} - \sum_{n=n_s}^{\infty}X_n^{(c)} + (p - \varepsilon^{(c)} + \varepsilon^{(d)})(X - X_1^{(c)}) \tag{A.41}$$

Eqs. (A.37) and (A.41) are identical with Eqs. (6.31) and (6.34) in the main text.

Appendix A.7. Estimation of n_s, L, V_{core} and n_M for perfluoroalkanes

To estimate the length of the surfactant molecules we calculated the length of both perfluoroalkanes (C_nF_{2n+2}) and normal alkanes (C_nH_{2n+2}) in vacuum using the ChemAxon software. Fig. A.2 shows the values calculated for C_nF_{2n+2} versus those for C_nH_{2n+2}. One sees that there is no significant difference between the lengths of the two types of chains at the same number of carbon atoms, n_C. Therefore, the Tanford formula for calculating the fully extended length of hydrocarbon chains can be used also for fluorocarbon chains. Thus, for the two investigated surfactants we obtain:

$$l = 0.154 + 8 \times 0.1265 \approx 1.17 \text{ nm} \quad \text{for} \quad \text{C8–TAC} \tag{A.42}$$

$$l = 0.154 + 12 \times 0.1265 \approx 1.67 \text{ nm} \quad \text{for} \quad \text{C12–TAC} \tag{A.43}$$

The diameter of the surfactant headgroup is $\delta_h = 0.69$ nm, as estimated by N.C. Christov et al., *Langmuir* **22** (2006) 7528–7542.

To obtain an expression for the volume of the surfactant tails, we evaluated the molecular volumes of fluorocarbon oils, v, by using the formula

$$v = \frac{M}{N_A\rho} \tag{A.44}$$

where N_A is the Avogadro constant, M is the molar mass, and ρ is the density of perfluoroalkane (see Table A.1).
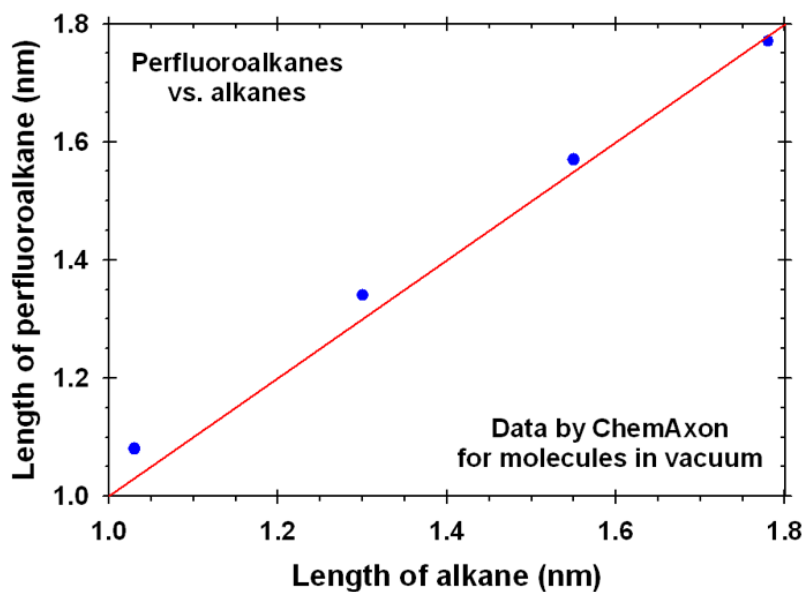
Fig. A.2. Comparison of perfluoroalkanes and normal alkanes with respect to their molecular length. The full circles correspond to molecules with 6, 8, 10 and 12 carbon atoms.

The calculated values of v depend linearly on n_C; see Fig. A.3. The fit with linear regression yields:

$$v = \left(51.8 + 46.0 n_C\right) \times 10^{-3} \text{ nm}^3 \tag{A.45}$$
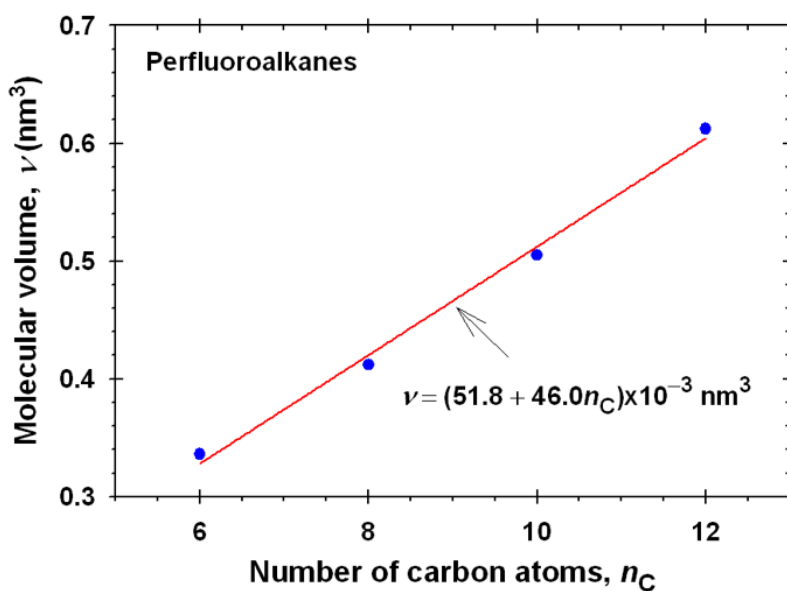
Fig. A.3. Dependence of C_nF_{2n+2} molecular volumes on the number of carbon atoms, n_C.

From Eq. (A.45) we obtain:

$$v = (51.8 + 46 \times 8) \times 10^{-3} = 0.420 \text{ nm}^3 \quad \text{for} \quad \text{C8–TAC} \tag{A.46}$$

$$v = (51.8 + 46 \times 12) \times 10^{-3} = 0.604 \text{ nm}^3 \quad \text{for} \quad \text{C12–TAC} \tag{A.47}$$

Table A.1. Molecular masses, densities and molecular volumes of perfluoroalkanes.

C_nF_{n+2}	M (g/mol)	ρ at 25 $^\circ$C (g/cm^3)	v (nm^3)
C_6F_{14}	338.04	1.669	0.336
C_8F_{18}	438.06	1.765	0.412
$C_{10}F_{22}$	538.07	1.770	0.505
$C_{12}F_{26}$	638.09	1.730	0.612

The aggregation number of a spherical micelle, n_s, is calculated as follows:

$$n_s = \frac{4\pi}{3} \frac{l^3}{v} \tag{A.48}$$

Using the obtained values for the molecular length l in Eqs. (A.42) and (A.43), and for the volume v in Eqs. (A.46) and (A.47), we obtain:

$$n_s = 16 \quad \text{for} \quad \text{C8–TAC} \quad \text{and} \quad n_s = 32 \quad \text{for} \quad \text{C12–TAC} \tag{A.49}$$

See Table 4 in the main article. Furthermore, L, V_{core} and the mass average aggregation number $\bar{n}_M$ are estimated from the experimental R_h and from v in Eqs. (A.46) and (A.47), using Eqs. (8.13) and (8.15) in the main article with $R = l$ and $b = l + \delta_h$, where the l values are given by Eqs. (A.42) and (A.43); see Table 3 in the main text.